The 8 June 1995 McLean, Texas, Storm. Part I: Observations of Cyclic Tornadogenesis

DAVID C. DOWELL*

NOAA/National Severe Storms Laboratory and Cooperative Institute for Mesoscale Meteorological Studies, Norman, Oklahoma

HOWARD B. BLUESTEIN

School of Meteorology, University of Oklahoma, Norman, Oklahoma

(Manuscript received 4 May 2001, in final form 18 April 2002)

ABSTRACT

On 8 June 1995 scientists participating in the Verification of the Origins of Rotation in Tornadoes Experiment (VORTEX) collected airborne Doppler radar data in a storm that produced a family of tornadoes near McLean, Texas. The Electra Doppler Radar (ELDORA) scanned three significant tornadoes during their formative and mature stages; one of the tornadoes was of F4/F5 intensity.

Evidence from pseudo-dual-Doppler analyses of the ELDORA data reveals a process of cyclic tornado formation qualitatively similar to that depicted in previous conceptual models. In particular, the rear-flank gust front appears to play a major role in determining the location of the next vortex in the series. When a tornado forms, a small region (3–5 km wide) of outflow surges ahead of the tornado, producing a local bulge in the gust front. A new vorticity maximum may form near the leading edge of the outflow. In contrast to what is suggested by earlier conceptual models, intersection of the rear-flank gust front with a wind shift along the forward flank does not appear to be a necessary element in the formation of the new vortex.

Previous studies have shown that if low-level outflow from the rear flank of a storm surges well ahead of the midlevel updraft, initiation of new deep, moist convection downshear along the gust front may be necessary for storm survival. In contrast, in the McLean storm, the rear gust front did not move ahead of the location of the midlevel updraft. The persistence of the main updraft may have fostered a rapid cyclic process.

The first and second tornadoes each, in short time, became separated from the main updraft. In contrast, the third large tornado in the family (the fourth overall) remained with the main updraft and persisted for over 1 h. Reasons for the transition of the cyclic phase into the long-lived phase will be discussed in Part II of this paper.

1. Introduction

The most violent tornadic storms tend to produce families of tornadoes, rather than just one tornado, often at strikingly regular intervals (Darkow and Roos 1970; Darkow 1971). Fujita et al. (1970) and Fujita (1974) documented these types of storms with detailed damage surveys and classified them according to patterns of tornado tracks. We will refer to the formation of a series of tornadoes in a supercell thunderstorm as ''cyclic tornadogenesis'' (Darkow and Roos 1970; Rasmussen et al. 1982).

In the Burgess et al. (1982) conceptual model for cyclic low-level vortex formation (Fig. 1), the configuration of the forward-flank and rear-flank boundaries in the thunderstorm resembles the frontal structure in a midlatitude synoptic-scale cyclone, as in the schematic of supercell structure by Lemon and Doswell (1979). Vortices repeatedly form at the occlusion point and dissipate as they become separated from the warm sector. In the Lemon and Doswell (1979) model, the storm that is producing a series of tornadoes is maintained by a series of discrete updrafts. Recently, Adlerman et al. (1999) provided a detailed description of the evolution of both low- and midlevel features in a numerical simulation of the cyclic formation of mesocyclones. The sequence of events at low levels in the simulation resembled that in the earlier conceptual models.

Until recently, documentation of cyclic tornadogenesis was limited to single-Doppler measurements (Burgess et al. 1982), dual-Doppler observations with relatively poor temporal and spatial resolution (Johnson et al. 1987), and visual records (e.g., Fujita et al. 1970; Rasmussen et al. 1982; Jensen et al. 1983; Bluestein et al. 1988; Davies et al. 1994). The quality of available

* Current affiliation: National Center for Atmospheric Research, Boulder, Colorado.

Corresponding author address: David C. Dowell, National Center for Atmospheric Research, P. O. Box 3000, Boulder, CO 80307-3000. E-mail: ddowell@ucar.edu

© 2002 American Meteorological Society

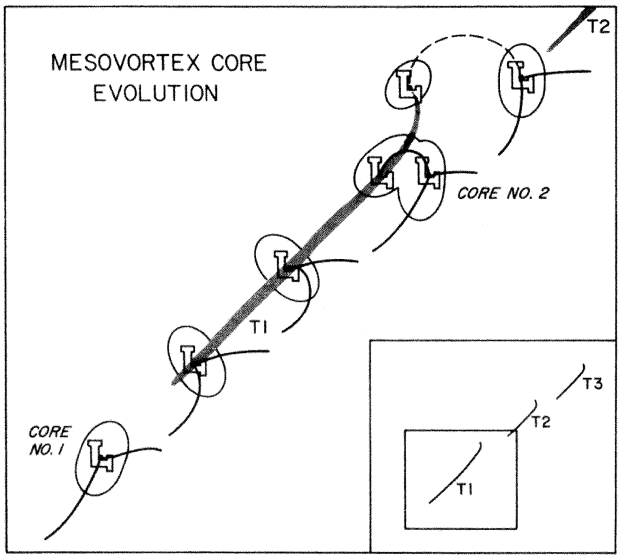

FIG. 1. Conceptual model of cyclic mesocyclone core formation (from Burgess et al. 1982). Tornado tracks are shaded, and thick lines represent forward-flank and rear-flank wind discontinuities. In the summary of the tornado tracks at the lower right, the smallest inset square corresponds to the expanded region in the figure.

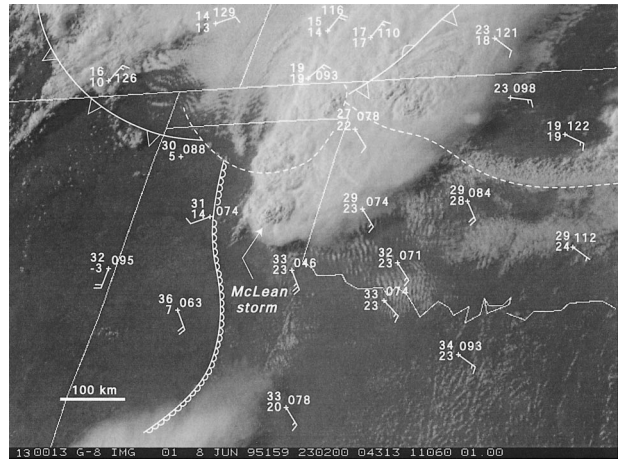

FIG. 2. Composite of surface analysis and *GOES-8* visible image centered on the eastern Texas Panhandle at 2300 8 Jun 1995. For each station, the temperature (upper left) and dewpoint (lower left) are in °C, and the altimeter setting (right) is in tenths of mb with leading ''10'' removed. Full (half) wind barbs represent 5 (2.5) m s^{-1}. The position of the front was estimated from the surface observations. Cloud features and surface observations provide evidence of the location of the old outflow boundary (dashed line) in central and northwest OK. In the northern Texas Panhandle, the new outflow boundary, which has overtaken the front, was associated with a fine line in the Amarillo, TX, WSR-88D images. The position of the dryline (scalloped line) was estimated from cloud features (faintly visible) and from the series of surface observations at sites in west Texas.

observations increased dramatically on 8 June 1995, the date of the last mission of the Verification of the Origins of Rotation in Tornadoes Experiment (VORTEX) (Rasmussen et al. 1994). In 1994 and 1995, VORTEX scientists collected datasets with airborne platforms, mobile ground-based platforms, and the operational suite of instruments in order to evaluate hypotheses of tornadogenesis and tornado dynamics. The primary data in our study are those collected with the Electra Doppler Radar (ELDORA) system on the National Center for Atmospheric Research (NCAR) Electra aircraft (Hildebrand et al. 1994; Wakimoto et al. 1996).

On 8 June 1995, several tornadic supercells formed in the Texas Panhandle (Fig. 2). The southernmost storm produced a family of tornadoes, some of them quite large, near McLean, Texas (Figs. 3 and 4). The ELDORA scanned this supercell (''the McLean storm'') from before the formation of the first tornado until well into the life of the fourth. Because convective clouds were absent to the south of the storm (Fig. 2), the Electra crew was able to obtain pseudo-dual-Doppler[1] (Jorgensen et al. 1996; Dowell et al. 1997) measurements at close range every 5–6 min by flying east–west-oriented legs to the south of the updraft.

Since the pseudo-dual-Doppler analyses of the McLean supercell are the first to document the cyclic formation of tornadoes at close range, we have taken advantage of this unique opportunity to evaluate the existing conceptual models of cyclic vortex formation in light of the new observations. In Part I of this study, we focus on qualitative aspects of the McLean storm, especially the morphology of the gust front and updraft in the tornadic region of the storm. We begin in section 2 by describing in more detail the case we have selected for intensive study. In section 3 and in an appendix, we describe the method used to synthesize the wind field from the ELDORA data and discuss what features could be resolved. In section 4, we compare the process of cyclic tornadogenesis depicted in our analyses to the prevailing conceptual models of cyclic tornadogenesis. Concluding comments are found in section 5. The quantitative analysis of cyclic tornado formation, maintenance, and dissipation is found in Dowell and Bluestein (2002, Part II of this paper).

2. The 8 June 1995 dataset

During the afternoon of 8 June 1995, storms formed progressively from north to south near the dryline in the Texas Panhandle (Fig. 2). VORTEX teams initially targeted a supercell in the eastern Oklahoma panhandle. However, when it became clear at 2200 UTC (all times hereafter given in UTC) that the initial storm was weakening, the teams focused their attention on tornadic storms farther south in the eastern Texas Panhandle.

First echoes on the lowest sweep of the Amarillo, Texas, Weather Surveillance Radar-1988 Doppler (WSR-88D) of the eventual target storm, hereafter de-

[1] Although the ELDORA is composed of two radars, we still refer to the data as ''pseudo-dual-Doppler'' since the synthesis involves observations that were collected from a single platform.

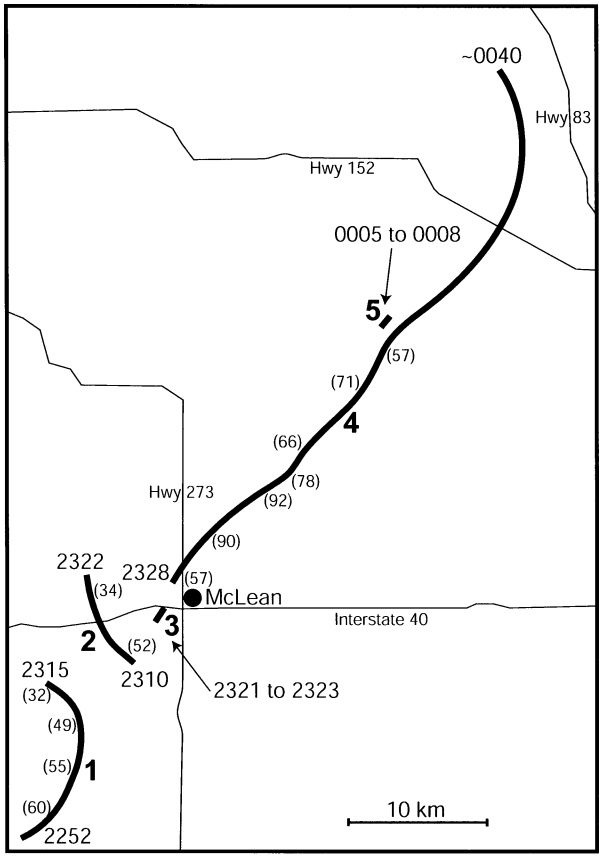

FIG. 3. Tornado tracks and local road network near McLean, TX, with approximate beginning and ending times (UTC on 8 and 9 Jun 1995) of the visible tornado condensation funnels. The numbers in parentheses are maximum edited ground-relative ELDORA single-Doppler wind speeds (m s^{-1}) below 2 km AGL in the tornadoes, during each aircraft pass.

noted the McLean storm, appeared approximately 12 km east of Silverton, Texas, at 2050 (not shown). The storm grew in size and intensity as it moved to the northeast. An instrumented National Oceanic and Atmospheric Administration (NOAA) P-3 aircraft and the NCAR Electra aircraft arrived after 2230, before the storm began to produce a family of at least five tornadoes (Figs. 3 and 4). By this time, the McLean storm was a large, high-reflectivity cell with a narrow appendage (Forbes 1981) on the southwest side (Fig. 5a). As was typical of the storms studied by Forbes (1981), the appearance of the first appendage on the southwest side of the storm at 2210 (not shown) preceded the formation of the first tornado by over 40 min.

Although the storm may be considered an isolated supercell, evidence from WSR-88D images of reflectivity (Fig. 5) indicates that this characterization is overly simplified. At 2247, a new low-level reflectivity feature appeared south of the McLean storm (Fig. 5b). This new feature (cell B) merged into the larger core of the main cell (A) (Figs. 5b–e) during the genesis of tornado 1. Raw ELDORA scans at 2249 (not shown) indicated neither reflectivity nor velocity characteristics of an active updraft with cell B. Apparently, the life cycle of the updraft that produced the precipitation was brief. Fallout of precipitation that had formed aloft was responsible for the increase in low-level reflectivity in cell B after 2249 (Figs. 5b–d).

After 2300, a trailing region of reflectivity began to develop southwest of the tornadic region (Figs. 5e–g), giving the storm an elongated appearance on its southwest side (Fig. 5f). In Part II of this paper, we will discuss the possibility of the interaction of cells along the flanking line with the main storm cell.

Other cells to the west and northwest of the McLean storm during much of its life (Fig. 5) organized into a companion supercell shortly before 0000 (Fig. 5i). The companion storm produced brief, weak tornadoes (R. Satkus 1995, personal communication). A third supercell (not shown) formed just east of the McLean storm and produced an F4 tornado near Allison, Texas, around 0100. Neither the companion storm nor the Allison storm is a focus of this study.

The ELDORA system scanned the McLean storm from an altitude of approximately 500 m AGL until 0015, when the pilots of the Electra aborted the mission after encountering extreme turbulence. For our study, we utilized primarily the data collected by the ELDORA during 17 east–west-oriented flight legs. [The center times of the aircraft passes are 2236, 2242, 2248, 2254, 2259, 2306, 2313, 2318, 2325, 2331, 2338, 2345, 2351, 2356, 0003, 0009, and 0015 (incomplete).] However, we also used in situ data from the P-3 aircraft and mobile-mesonet surface data (Straka et al. 1996) collected when ground teams arrived during the mature stage of tornado 4.

Our estimates of the times of the tornadoes (Fig. 3) are from video documentation. Tornadoes 3 and 5 were narrow and brief (Figs. 4c and 4d); the others (especially tornado 4) were large (with condensation funnels exceeding 700 m in width in each case) and long lived (Figs. 4a, 4b, and 4d). Tornado 4 was obscured by rain after 0030, so we know little about its late evolution. The Amarillo, Texas, National Weather Service (NWS) office rated the damage (Fujita 1981) in tornadoes 3 and 5 as F0, tornadoes 1 and 2 as F2, and tornado 4 as F4[2] (NCDC 1995). The maximum low-level (below 2 km AGL) Doppler wind measurements by the ELDORA in the first two significant tornadoes (Fig. 3) lie within the range of wind speeds Fujita (1981) associated with F2 damage. The wind speed of 92 m s^{-1} in tornado 4 (Fig. 3) is at the threshold between wind speeds associated with F3 and F4 tornadoes. A more detailed comparison of wind speeds to damage ratings is not possible for this case for several reasons. First, relatively few homes were affected by the McLean storm tornadoes. Second,

[2] R. Wakimoto (1995, personal communication) based on an exhaustive ground and aerial survey, rated the damage of tornado 4 as F5.

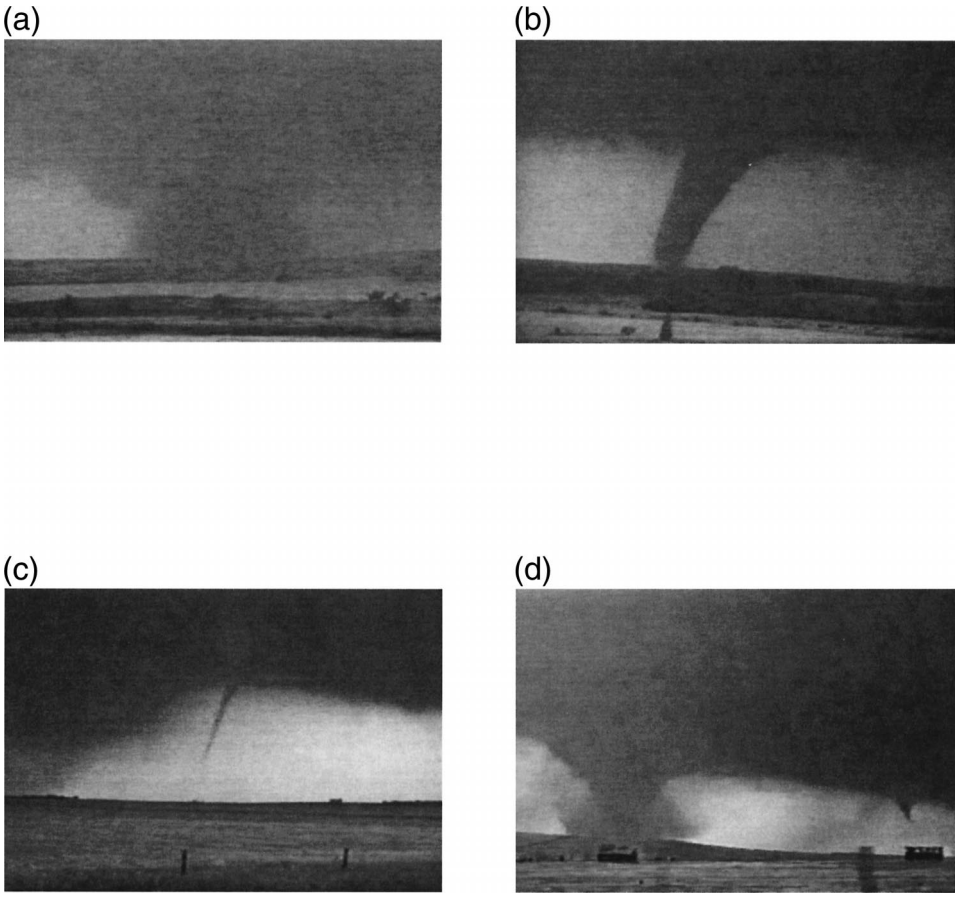

FIG. 4. Video frames of the McLean storm tornadoes. (a) Tornado 1 to west-northwest at 2302 UTC. (Copyright 1995 by B. Haynie.) (b) Tornado 2 to northwest at 2312 UTC. (Copyright 1995 by B. Haynie.) (c) Tornado 3 to northwest at 2321 UTC. (Copyright 1995 by B. Haynie.) Tornado 2 (not visible in this image) was to the left of tornado 3 from this viewing location. (d) Tornado 4 (left) and tornado 5 funnel cloud (right) to west at 0008 UTC. (VORTEX video by C. Kaufman.)

the ELDORA measurements within ~500 m of the surface are contaminated by ground clutter. Third, features in the wind field on scales of a few 100 m or less are not resolved in the ELDORA data.

Ground teams were not in position to obtain an environmental sounding near the McLean storm. We have combined data from multiple sources to estimate the environmental conditions south of the updraft of the mature storm (Fig. 6). The surface observations are from mobile-mesonet vehicles (Straka et al. 1996) that were 25 km south-southeast of the updraft at 2350. The observations between 0.5 and 3.5 km AGL are in situ measurements collected from the P-3 while it descended during a turn approximately 30 km south of the updraft at 2240. Thermodynamic measurements at upper levels (i.e., above 3.5 km AGL) are from a sounding at 2300 from Amarillo, Texas, which is 110 km west of McLean. To estimate the upper-level winds, we computed the mean wind at each grid level in a pseudo-dual-Doppler analysis of ELDORA data collected 60 km east-northeast of the storm at 2225. Although features in the sounding at the interfaces between data types could be related to spatial and temporal variability of the environment, we note that in a region of data overlap between 2.0 and 3.5 km AGL, the ELDORA wind (Amarillo temperature) measurements were within 4 m s^{-1} (1 K) of those obtained from the P-3. Since the low- and mid-level wind measurements were collected within 30 km of a mature updraft, the profile may have been modified by the storm itself (Dowell and Bluestein 1997; Markowski et al. 1998; Weisman et al. 1998).

An unusually high surface dewpoint (22°–23°C) for the Texas Panhandle in early June contributed to a very high value of CAPE of 5380 J kg^{-1} (Fig. 6). The bulk Richardson number was 36, which is in the range that supports simulated supercells (Weisman and Klemp 1982, 1984). Particularly noteworthy in the wind profile is the high magnitude of the vertical shear of the horizontal wind (0.8×10^{-2} s^{-1}) from 3 m to 3 km AGL. In addition, the hodograph indicates a significant change in direction of the shear vector from near the surface to above the boundary layer (Wicker 1996). Since there

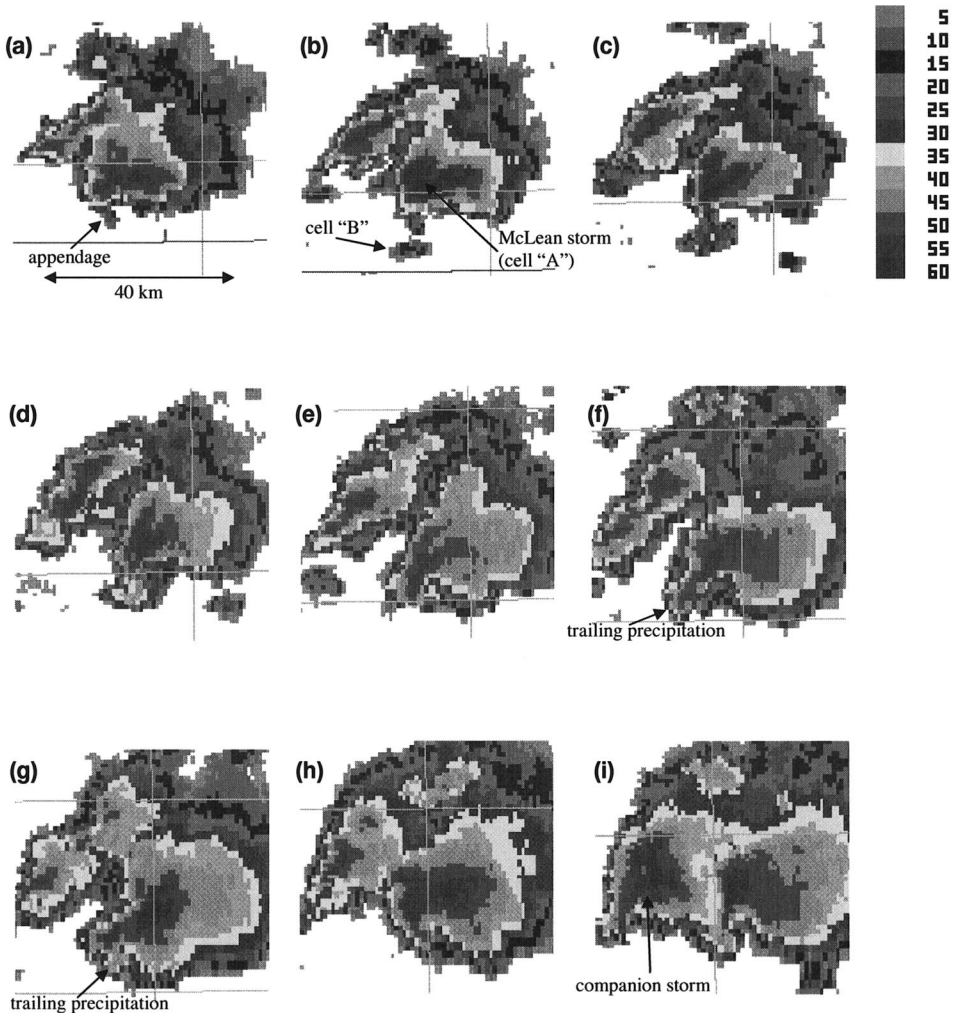

FIG. 5. Reflectivity factor (dBZ_e, with scale shown on the right) at 0.5° elevation angle from the Amarillo, TX, WSR-88D on 8 Jun 1995. The storm was approximately 100 km east of the radar site. If a tornado was observed at the time of the image, then this is noted in parentheses after the time: (a) 2238, (b) 2247, (c) 2252 (tornado 1), (d) 2257 (tornado 1), (e) 2307 (tornado 1), (f) 2317 (tornado 2), (g) 2327, (h) 2342 (tornado 4), and (i) 2357 UTC (tornado 4).

is a large vertical distance between the mesonet observation at 3 m and the lowest P-3 measurement at 500 m AGL, we examined Doppler measurements from the ELDORA in order to resolve better the shape of the low-level hodograph. Pseudo-dual-Doppler wind syntheses from clear air data within 3 km of the flight track were possible for levels as low as 50 m AGL. The hodograph that was derived from ELDORA data ~15 km south-southeast of the main storm updraft at 2259 indicates stronger low-level winds (Marwitz and Burgess 1994) than those observed during the more distant P-3 descent (Fig. 6b). There is evidence of a turn in the hodograph toward the origin below 200 m AGL. At 2259, most of the decrease in the boundary layer wind speed toward zero at the ground apparently occurred within the lowest 50 m.

3. Pseudo-dual-Doppler analysis

Fore and aft scanning by the two antennas in the ELDORA allows one to collect pseudo-dual-Doppler (Jorgensen et al. 1996; Dowell et al. 1997) data with a between-beam angle of 35°–40° (Wakimoto et al. 1996). The radar transmits at two different pulse-repetition frequencies (Sirmans et al. 1976), giving an effective unambiguous velocity (± 78.7 m s^{-1}) suitable for the study of severe convection (Wakimoto et al. 1996). For typical Electra flight speeds (120 m s^{-1}) and antenna rotation rates (133° s^{-1}) during convective-mode scanning, the along-flight-track spacing between consecutive sweeps is ~300 m. This spacing is comparable to the beamwidth, which was 160–470 m at ranges of 5–15 km to the McLean tornadoes.

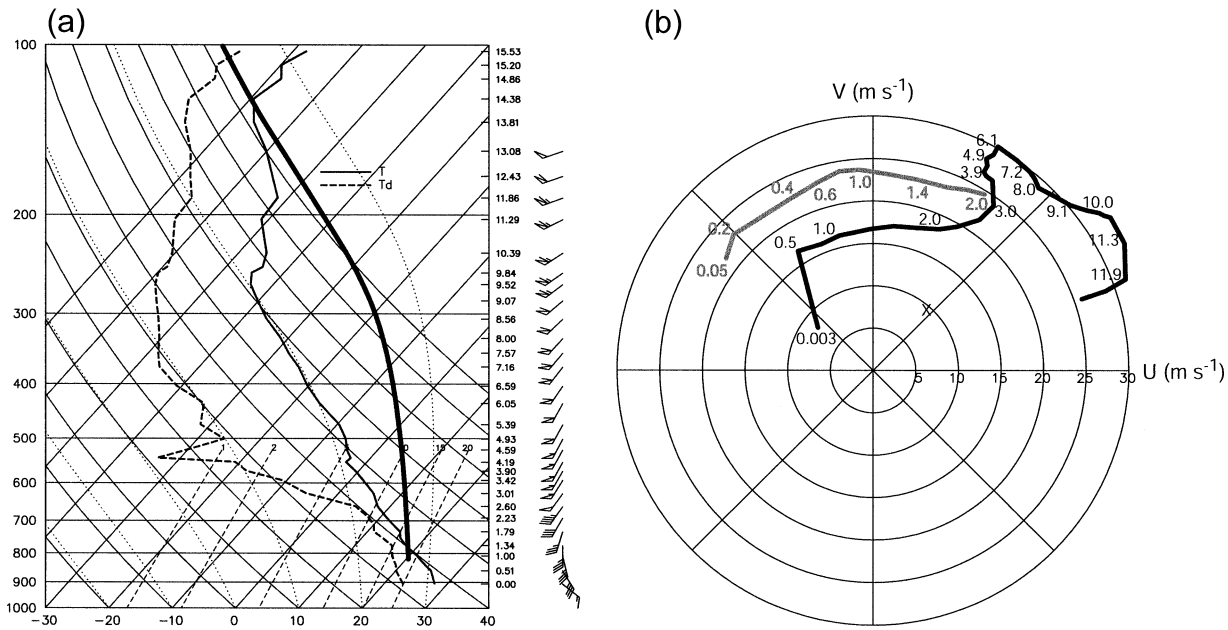

FIG. 6. Environmental conditions near the McLean storm. (a) Estimated sounding (details given in the text) ~30 km south of the McLean storm updraft at 2300 UTC 8 Jun 1995. Temperatures (T) and dewpoints (T_d) (bottom) are in °C, pressures (left) are in mb, and heights (right) are in km AGL. The heavy line on the sounding is a pseudoadiabatic ascent curve for a parcel with the mean properties of the lowest 500 m of the sounding. CAPE (computed based on virtual temperature without condensate loading) is 5380 J kg^{-1}. Wind barbs and flags represent 10 kt (≈5 m s^{-1}) and 50 kt (≈25 m s^{-1}), respectively. (b) Hodograph corresponding to the sounding in (a) (dark line) and hodograph synthesized from ELDORA clear air data near the flight track 15 km south-southeast of the McLean storm updraft at 2259 UTC (gray line). The rings are at 5 m s^{-1} intervals. Heights are in km AGL. Mean storm motion is indicated by the X in the hodograph.

We describe the variational method used to analyze the ELDORA pseudo-dual-Doppler measurements in the appendix. The wind syntheses resolve features as small as 2–3 km in width/height every 5–6 min. We refer the reader to Doviak et al. (1976), Ray et al. (1980, 1985), Jorgensen et al. (1983), Hildebrand and Mueller (1985), Ray and Stephenson (1990), and Wakimoto et al. (1998) for general discussions of errors in ground-based and airborne dual-Doppler analyses. Perhaps the primary challenge in diagnosing tornadogenesis with the ELDORA data is the lack of measurements near the surface. For typical ranges to the tornadoes in this particular case, we determined that the winds below approximately 500 m AGL were contaminated by ground clutter. As described in the appendix, we specified 500 m as the lowest level in the grid and assumed that divergence measurements at that level were representative of the entire layer below. The lack of wind measurements near the surface represents a significant source of error owing to the typical presence of strong velocity gradients in both the horizontal and vertical in supercell and tornado boundary layers (Lewellen 1993; Wurman et al. 1996; Dowell and Bluestein 1997). Other sources of uncertainty for this particular case relate to temporal sampling. Storm evolution between the times of the fore and aft measurements at a particular point introduces error into the analysis. At ranges of 5–15 km, the observations are separated in time by 30–90 s. In addition, the 5–6-min time between consecutive pseudo-dual-Doppler volumes makes it difficult to follow the evolution of individual storm features.

In this paper, we focus primarily on the relationship of the tornadoes to the parent storm. To determine the locations of the tornadoes for the figures, we identified the locations (relative to the dual-Doppler grid origin) of the tornado signatures in the raw ELDORA scans. Tornadoes are associated with strong cyclonic shear in Doppler velocity (e.g., Fig. 7a) and weak-echo holes in reflectivity (Fig. 8) (Fujita 1981; Wakimoto et al. 1996). (As discussed in the appendix, centrifuging of scatterers by the tornadoes, which likely produced the observed minima in reflectivity, could be an additional source of error in the wind synthesis.) Bounded weak-echo regions associated with updrafts in the McLean storm were sometimes as narrow as those of the tornadoes (not shown), but the updraft signatures were distinguishable from the tornado signatures by the lack of sharp cyclonic shear. The tornado signatures extended from the surface to over 13 km AGL (e.g., Fig. 8b) in some cases. We also verified the locations of the radar signatures against known points of damage at the ground.

In the case of tornado 4 at 0003, which the radar scanned from a range of 5 km, the dual-Doppler analysis indicates a vorticity maximum 0.5 km north-northwest of the tornadic shear signature (Burgess et al. 1975) in the single-Doppler winds (Fig. 7a). The broader-scale wind pattern was apparently asymmetric about the tor-

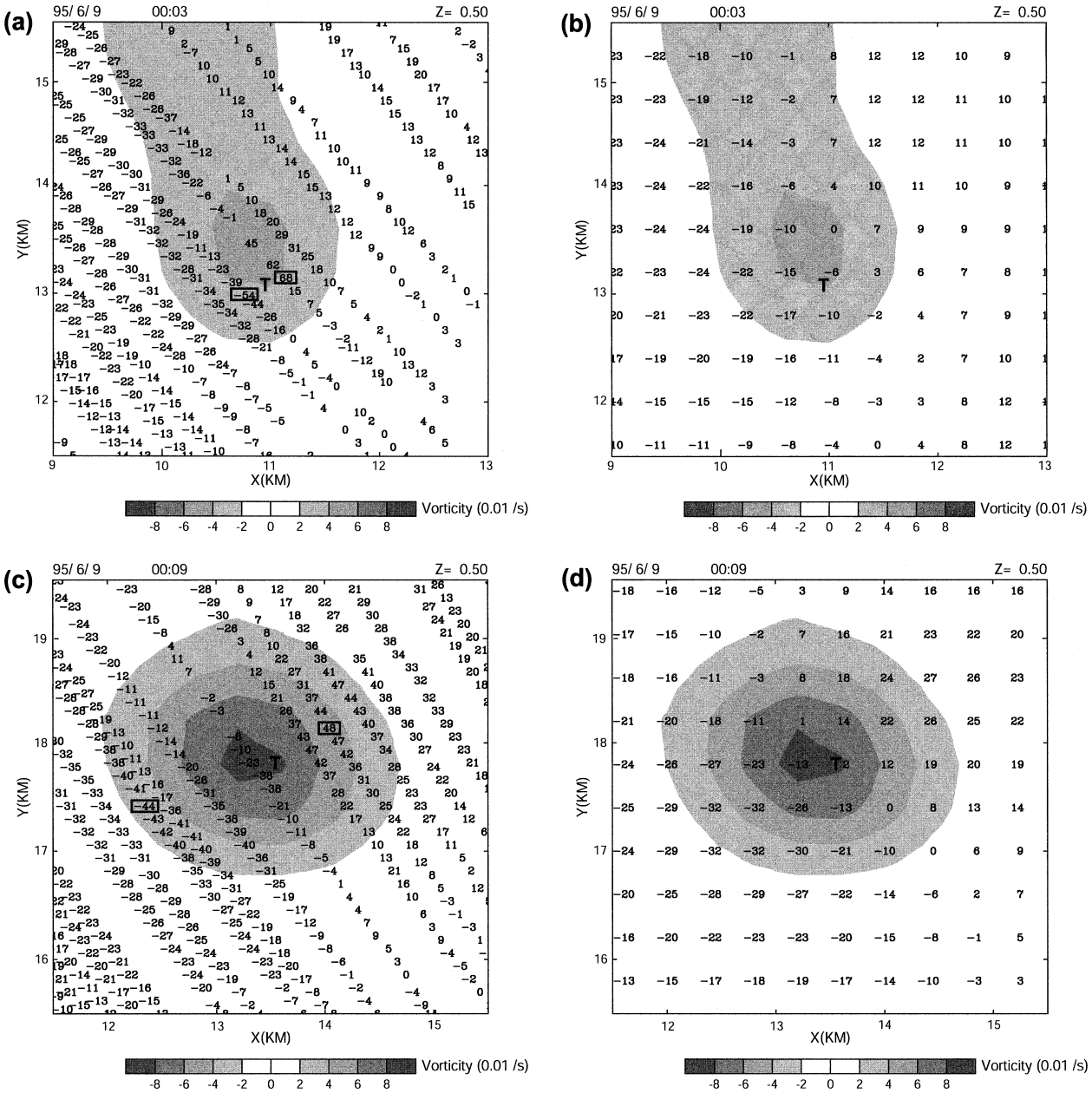

FIG. 7. Vertical vorticity (shading at intervals of 0.01 s^{-1}) in the pseudo-dual-Doppler analyses at 0.5 km AGL. The *x* and *y* distances (km) are relative to McLean. The approximate location of the center of tornado 4 is indicated by the letter T. (a) The edited radial velocity values (m s^{-1}) from the fore radar at 0003 UTC 9 Jun 1995. The radar was scanning toward the northwest while the plane flew west-southwest. Positive (negative) values indicate flow away from (toward) the radar. (b) The horizontal velocity component from the southeast (m s^{-1}) in the pseudo-dual-Doppler analysis at 0003 UTC 9 Jun 1995. (c) The edited radial velocity values (m s^{-1}) from the aft radar at 0009 UTC 9 Jun 1995. The radar was scanning toward the northwest while the plane flew east-northeast. (d) The horizontal velocity component from the southeast (m s^{-1}) in the pseudo-dual-Doppler analysis at 0009 UTC 9 Jun 1995.

nado. At most of the other times for this case, the resolved vorticity maxima were closer to the locations of the tornadoes. The high wind speeds in the raw data (68 m s^{-1} outbound and 54 m s^{-1} inbound in Fig. 7a) are not discernible in the dual-Doppler synthesis (Fig. 7b).

At some of the other times during the life of tornado 4 (e.g., 0009), the distance between the locations of the peak inbound and outbound radial velocities was greater (Fig. 7c). Although the peak velocity magnitudes were not as high as at the previous time (Fig. 7a), there had been a significant increase in the areal coverage of high wind speeds (e.g., the large area of outbound velocities greater than 20 m s^{-1} in Fig. 7c). The dual-Doppler analysis (Fig. 7d) thus indicates stronger winds and

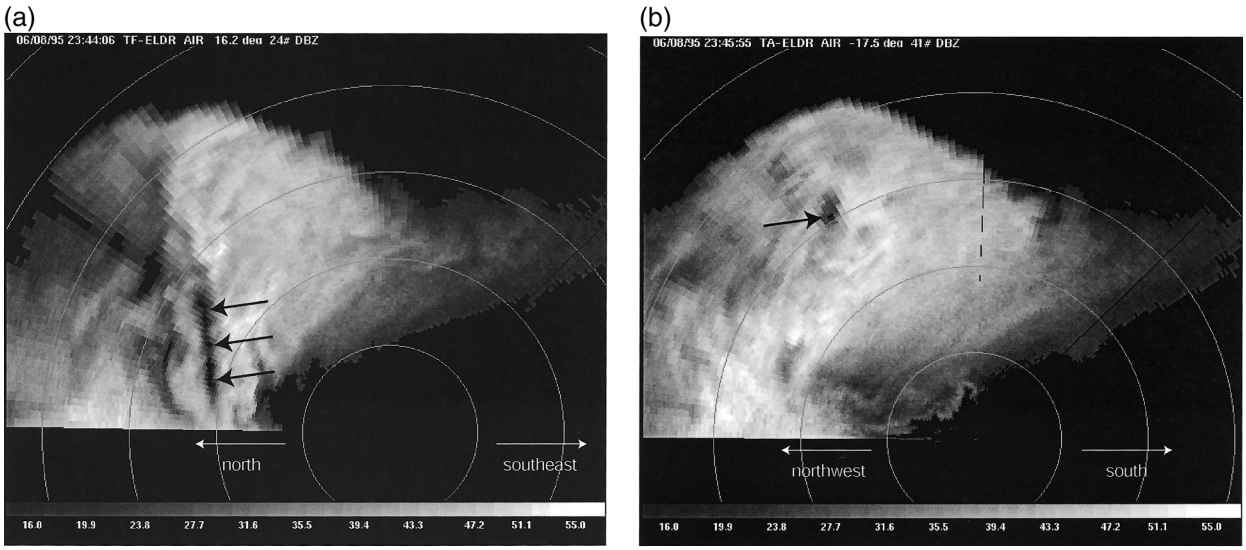

FIG. 8. Edited scans of reflectivity factor (dBZ_e, scale indicated at bottom of each image) by the ELDORA. The roughly cone-shaped scans have been projected onto a flat surface; the beam orientations at low levels are indicated. The range rings are at 5-km intervals, and the radar is located at the center of the rings. The locations of reflectivity minima associated with tornado 4 are indicated by arrows. (a) Scan by the fore radar at 2344:06 UTC. The slice through the tornado at midlevels is approximately vertical. (b) Scan by the aft radar at 2345:55 UTC. Since both the ELDORA sweep and the tornado are tilted at upper levels, the slice is nearly perpendicular to the axis of the tornado.

higher values of vorticity than at the previous time (Fig. 7b). The dual-Doppler syntheses may be used to evaluate the strength of the flow in the vicinity of the tornado on scales of 2–3 km or more but should not be used to evaluate tornado intensity. Although tornado-scale information present in some of the close scans of the large tornadoes is removed by the objective analysis and wind synthesis, the use of the spatially and temporally uniform wind retrieval method allows for an unambiguous assessment of the evolution of the larger-scale features (Trapp and Doswell 2000).

4. Comparison to conceptual models

a. Low-level wind and temperature

1) BACKGROUND

Usage of terms such as ''mesocyclone'' and ''tornado cyclone'' is inconsistent in previous descriptions of low-level vortices in supercells. In this section, we will adhere to the convention that mesocyclones refer to vortices that are 2–10 km wide (Glickman 2000, 484–485). Agee et al. (1976) suggested that some supercell mesocyclones (called tornado cyclones in the original text) contain multiple long-lived sub-mesocyclone-scale vortices (1–3 km wide, termed mini tornado cyclones) that revolve more than once about the mesocyclone center. In their conceptual model, a tornado forms when the sub-mesocyclone-scale vortex strengthens in the warm sector of the larger-scale circulation, and the tornado dissipates when the parent vortex passes through the region of cold storm outflow. Agee et al. (1976) developed this conceptual model in order to explain cycloidal tornado tracks in the ''super-outbreak'' of 3 April 1974.

In the Burgess et al. (1982) description of storm structure, the broad region of cyclonic swirl in the storm (which may be up to 20 km wide) contains one or more embedded regions of approximately solid-body rotation (termed mesocyclone cores in the text) (Fig. 1). Since these embedded vortices were 4–6 km wide in the observations, we will apply the term mesocyclones in the discussion below. In their extensive dataset of single-Doppler radar observations, Burgess et al. (1982) found that 24% of supercells developed more than one mesocyclone. The mesocyclones observed on radar were often associated with tornadoes.

The Burgess et al. (1982) conceptual model for low-level evolution in cyclic supercells (Fig. 1) builds on earlier explanations by Lemon and Doswell (1979). During the mature stage of the first tornado, a gust front wraps cyclonically about the right side of the tornado (where directions described are relative to a viewer looking in the direction toward which the tornado's parent storm is moving). Eventually the rear-flank gust front wraps around far enough to form an occlusion with the forward-flank gust front. The supply of warm environmental air to the mesocyclone is cut off, and the occluded mesocyclone turns to the left and weakens. The occluded vortex eventually dissipates completely, rather than strengthening again at a later time as in the Agee et al. (1976) model.

While the first low-level mesocyclone dissipates, a second mesocyclone develops rapidly in the region of strong convergence at the occlusion point of the storm-

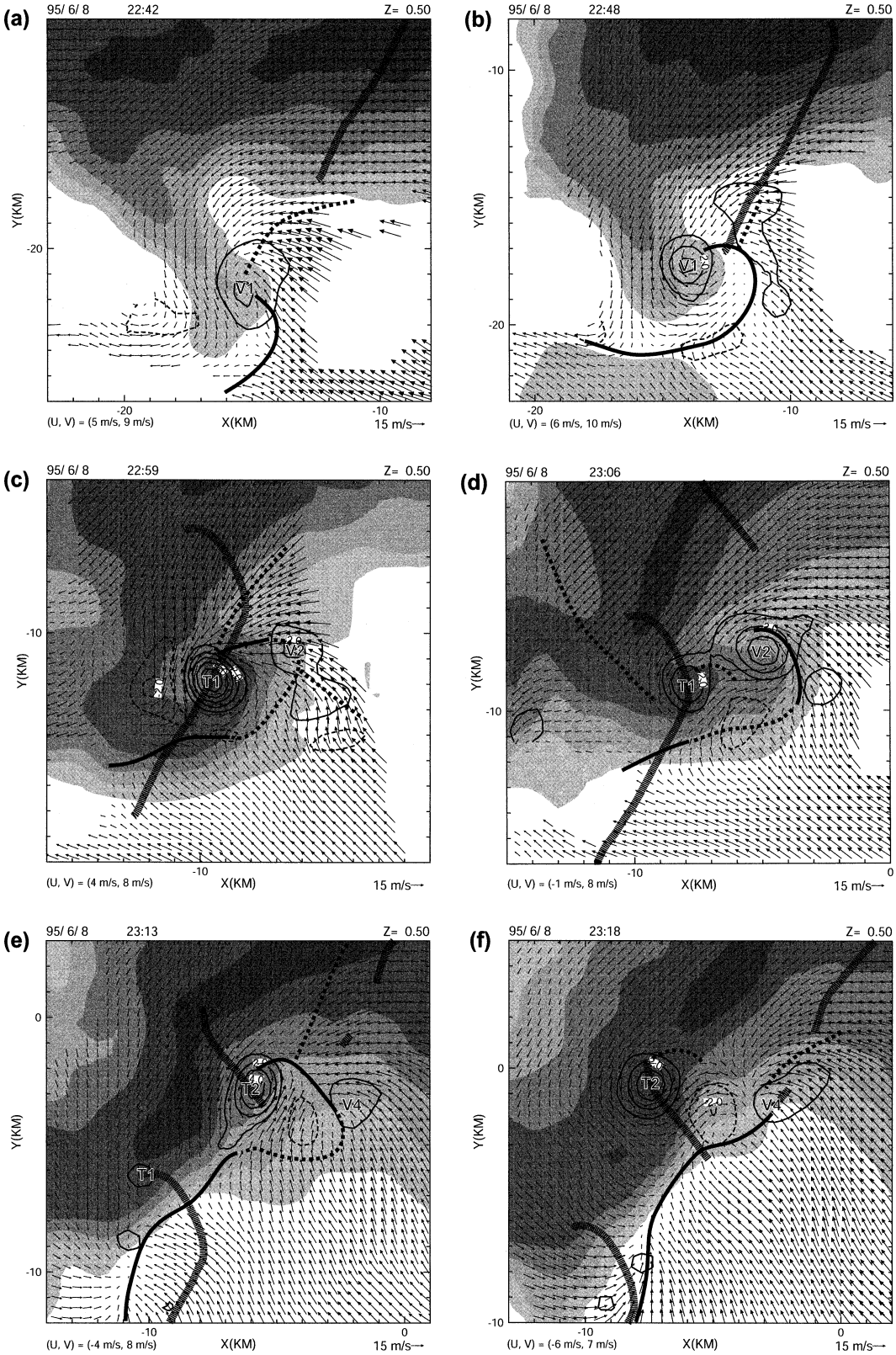
(a)
95/ 6/ 8 22:42 Z= 0.50
Y(KM)
-20
V1
-20
-10
(U, V) = (5 m/s, 9 m/s)
X(KM)
15 m/s
(b)
95/ 6/ 8 22:48 Z= 0.50
-10
Y(KM)
V1
V2
-20
-20
-10
(U, V) = (6 m/s, 10 m/s)
X(KM)
15 m/s
(c)
95/ 6/ 8 22:59 Z= 0.50
-10
Y(KM)
V2
T1
-10
(U, V) = (4 m/s, 8 m/s)
X(KM)
15 m/s
(d)
95/ 6/ 8 23:06 Z= 0.50
Y(KM)
V2
T1
-10
-10
0
(U, V) = (-1 m/s, 8 m/s)
X(KM)
15 m/s
(e)
95/ 6/ 8 23:13 Z= 0.50
0
Y(KM)
T2
V4
T1
-10
-10
0
(U, V) = (-4 m/s, 8 m/s)
X(KM)
15 m/s
(f)
95/ 6/ 8 23:18 Z= 0.50
0
Y(KM)
T2
V4
-10
-10
0
(U, V) = (-6 m/s, 7 m/s)
X(KM)
15 m/s

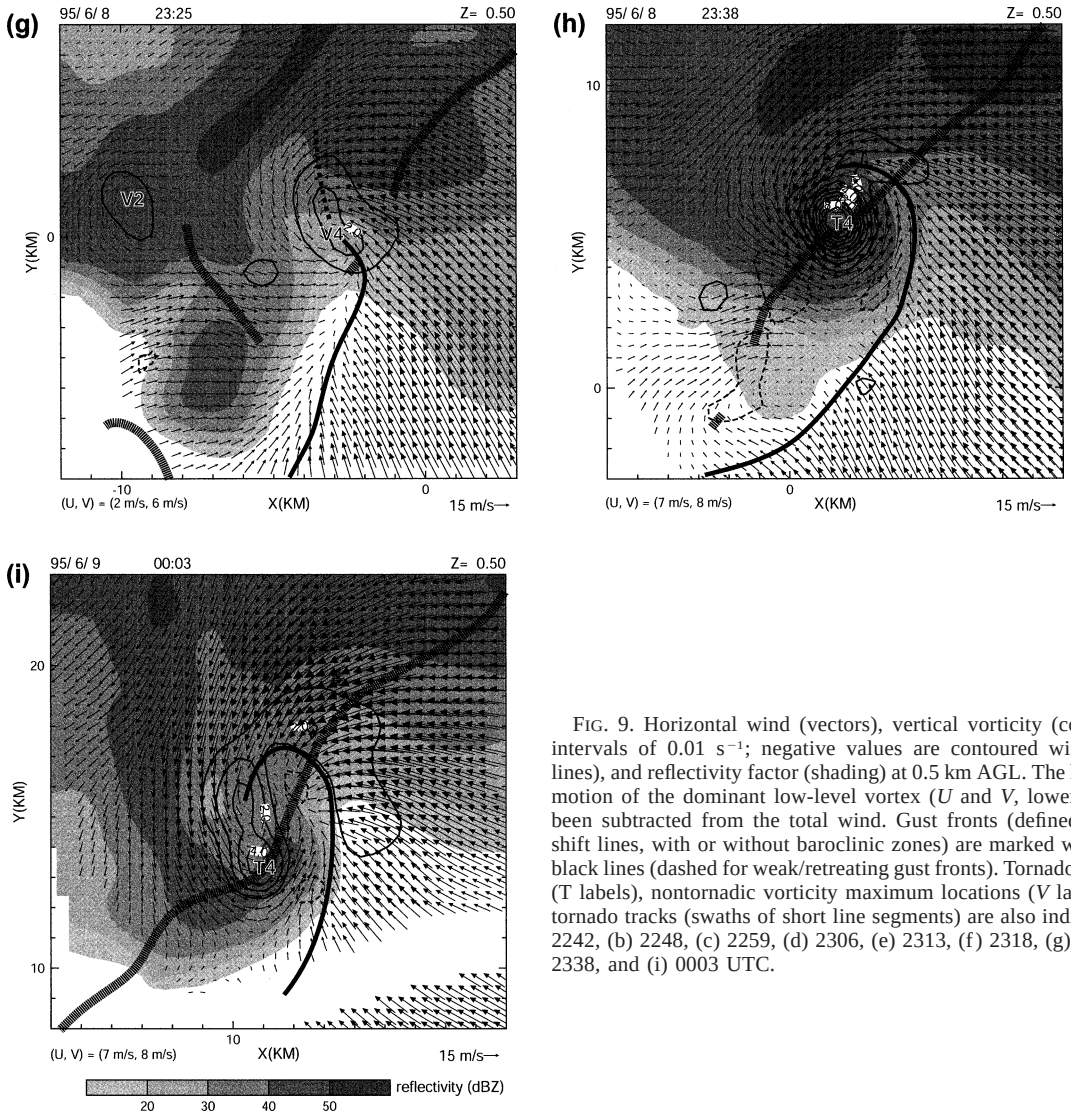

FIG. 9. Horizontal wind (vectors), vertical vorticity (contours at intervals of 0.01 s^{-1}; negative values are contoured with dashed lines), and reflectivity factor (shading) at 0.5 km AGL. The horizontal motion of the dominant low-level vortex (*U* and *V*, lower left) has been subtracted from the total wind. Gust fronts (defined as wind shift lines, with or without baroclinic zones) are marked with heavy black lines (dashed for weak/retreating gust fronts). Tornado locations (T labels), nontornadic vorticity maximum locations (*V* labels), and tornado tracks (swaths of short line segments) are also indicated: (a) 2242, (b) 2248, (c) 2259, (d) 2306, (e) 2313, (f) 2318, (g) 2325, (h) 2338, and (i) 0003 UTC.

scale boundaries (Fig. 1). Unlike the first low-level mesocyclone, which formed rather slowly following mid-level mesocyclogenesis, the new mesocyclone forms rapidly and simultaneously over a large depth because it is in a region that is rich in vertical vorticity (i.e., within the broad region of cyclonic swirl). The new mesocyclone, which may be associated with a tornado, becomes dominant until its associated gust fronts occlude and the next vortex cycle is initiated in a similar manner.

Visual observations support some aspects of the Burgess et al. (1982) conceptual model. Rasmussen et al. (1982) and Jensen et al. (1983) observed gust front surges ahead (to the east) of existing tornadoes and noted that the new tornado began to form near this location (Bluestein et al. 1988) when the surge slowed. The sequence of events in the Burgess et al. (1982) model also resembles that in the numerical thunderstorm simulation by Adlerman et al. (1999). A noteworthy difference is that ambient vertical vorticity was not necessary for cyclic vortex formation in the simulations; instead, new vortices formed in a manner similar to that of the first vortex. Another difference is in the gust front structure. Burgess et al. (1982) specifically described the boundary along the forward flank (extending eastward from the vortex) as a wind discontinuity (Fig. 1). However, neither the recent numerical simulation by Adlerman et al. (1999) nor earlier simulations (e.g., Rotunno and Klemp 1985) indicated a prominent wind shift along the forward flank. Instead, the authors of the numerical simulation studies defined the gust front structure in terms of the temperature field. In the simulations, the low-level baroclinic zone was roughly north–south oriented both north and south of the mesocyclone, was curved (S shaped) in the mesocyclone region, and was generally sharpest just behind the rear-flank wind shift.

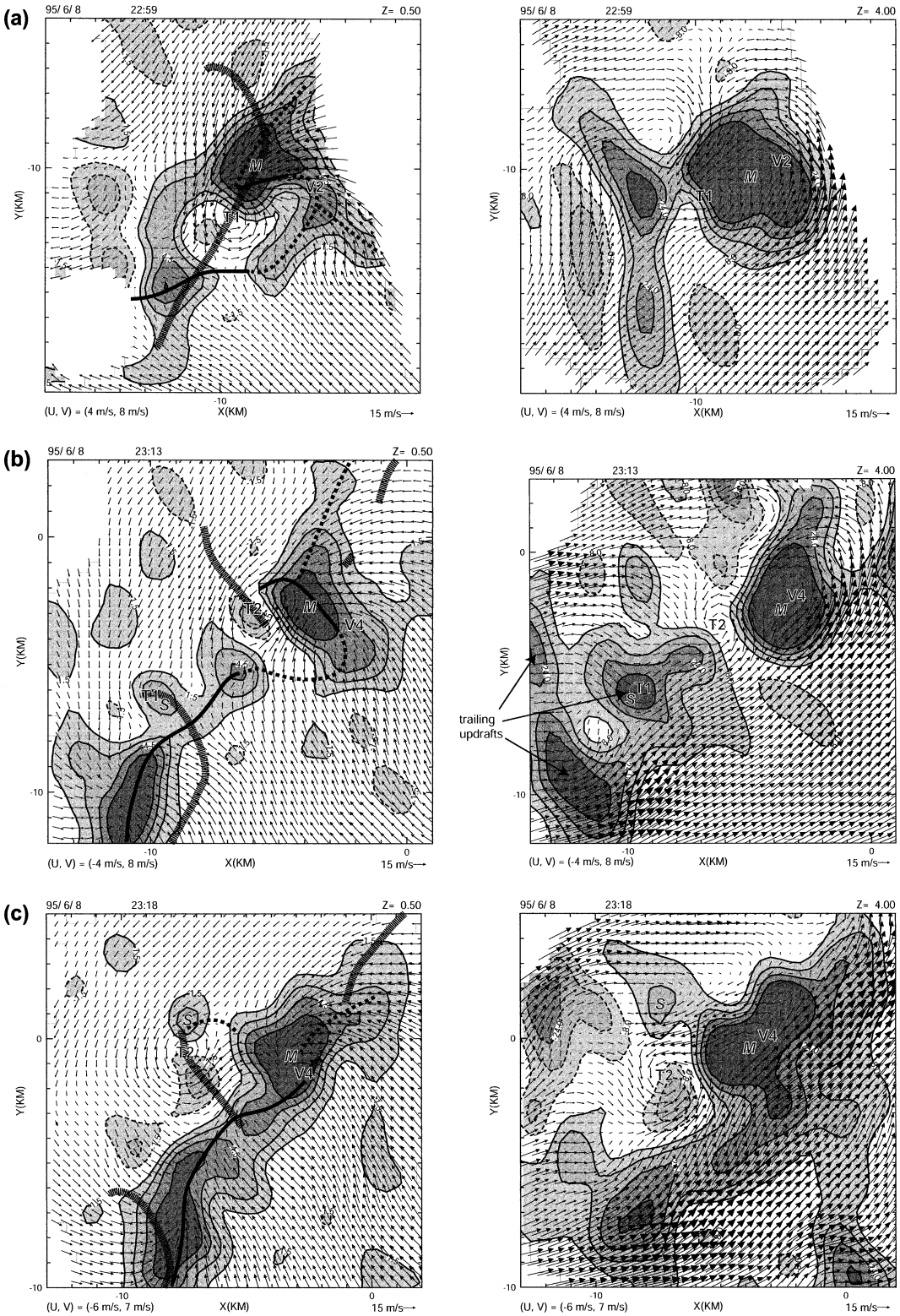

FIG. 10. Horizontal vortex-relative wind (vectors) and vertical velocity (shading and contours; negative values are contoured with dashed lines), at 0.5 km AGL (left) and 4.0 km AGL (right). The contour intervals for vertical velocity are 1.5 and 8.0 m s^{-1} at 0.5 and 4.0 km AGL, respectively. Other labels, etc., are as in Fig. 9 or as described in the text: (a) 2259 UTC, (b) 2313 UTC, 14 min after previous panel, (c) 2318 UTC, 5 min after previous panel, (d) 2325 UTC, 7 min after previous panel, (e) 2338 UTC, 13 min after previous panel, and (f) 0009 UTC, 31 min after previous panel.

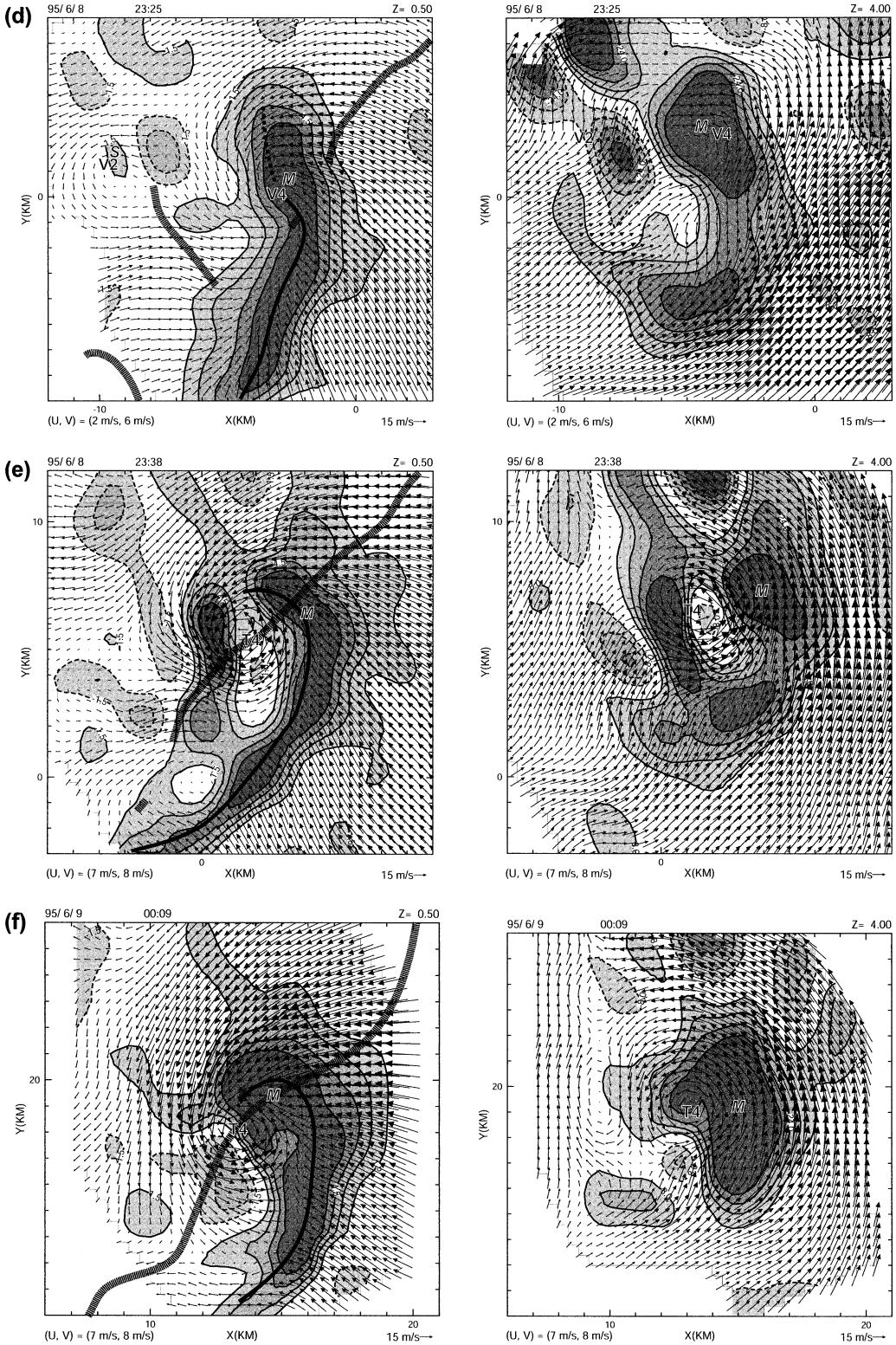

FIG. 10. (*Continued*)

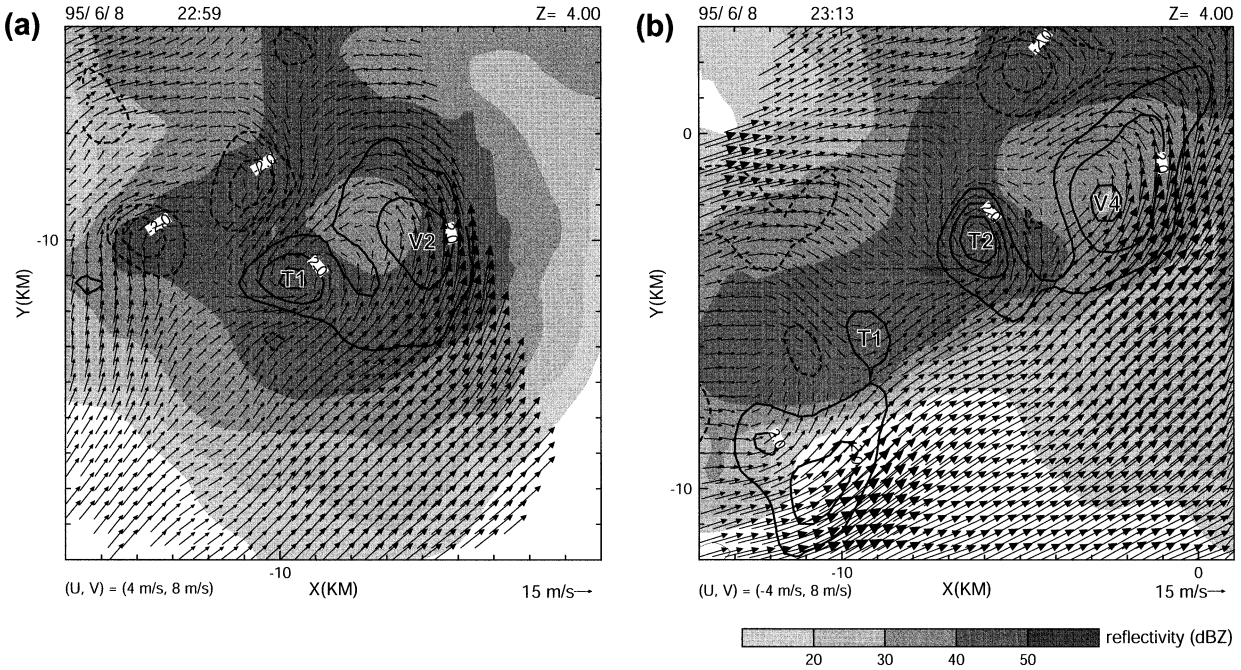

FIG. 11. As in Fig. 9, but at 4.0 km AGL: (a) 2259 and (b) 2313 UTC.

2) OBSERVATIONS OF THE MCLEAN STORM

In the descriptions of the McLean storm, we will use phrases such as ''resolved vorticity maxima'' to describe the vortices in the pseudo-dual-Doppler analyses that appear to be larger than tornadoes. The resolved vorticity maxima (regions where vertical vorticity exceeds 0.01 s^{-1}) are 1–3 km wide (e.g., Fig. 7). This size is slightly smaller than what is typically associated with a mesocyclone (2–10 km wide) (Glickman 2000, 484–485) but larger than what is typically associated with a tornado (1 km or narrower) (Fujita 1981). Evidence in most of the raw ELDORA observations indicates that the actual vortices (identified by their couplets of local maxima and minima in radial velocity) are significantly narrower than the width of the vorticity maxima in the dual-Doppler syntheses (e.g., Fig. 7a).

For the comparison of our analyses to features in the conceptual models, we will rely on many analyses at 500 m AGL (e.g., Fig. 9), the approximate lowest level with pseudo-dual-Doppler data uncontaminated by ground clutter. The horizontal winds depicted in Figs. 9–11 are relative to the motion of the dominant low-level vortex at the time of each analysis. Since there were turns in the tracks of the vortices (Fig. 3), the reference-frame motion changes from one time to the next. This choice of reference frame allows one to interpret better the kinematic features in the vicinity of the vortices but could make it more difficult for one to evaluate the evolution of flow characteristics away from the vortices.

In general, the analyses of the McLean storm are qualitatively consistent with the Burgess et al. (1982) model in terms of rear-flank gust front behavior and the relative locations of vortices. The notation in the figures (e.g., Fig. 9) is consistent with that in Burgess et al.'s (1982) diagram (Fig. 1); that is, ''gust front'' symbols identify features in the wind field. (Since few temperature measurements are available in this case, we are able to identify wind shifts more easily than baroclinic zones.) We generally analyzed the rear-flank gust front along lines of low-level convergence, that is, through relative maxima of low-level upward motion (Fig. 10). In regions of neutral vertical motion where we have indicated a continuous gust front, we identified weak wind shifts (not associated with significant upward motion), and we also considered the location of the gust front at the previous and next analysis times. For example, the portion of the rear-flank gust front to the southwest of vortex 2 (V2) at 2259 is drawn through a narrow region of updraft (Fig. 10a). The location of this subtle portion of the boundary is also consistent with the earlier location of the bow in the gust front (Fig. 9b). The dashed nature of the line at 2259 (Figs. 9c and 10a) indicates that this portion of the boundary is weak and could be retreating (i.e., there is rearward vortex-relative flow on each side of the boundary). The analysis of the location of forward-flank boundaries is more subjective. In Figs. 9 and 10, we have noted with dashed lines subtle boundaries, when present, along the forward flank, generally to the north and northeast of the vorticity maxima.

Analyses from the first three aircraft passes near the storm (examples from the second and third passes shown in Figs. 9a and 9b) indicate an intense low-level cir-

culation (V1), which we have identified as pretornadic. Although a definitive classification of a low-level vortex as either tornadic or nontornadic is not always possible, we note that vortex 1 was associated with a visible condensation funnel, Doppler wind speeds in excess of 35 m s^{-1}, and damage near the surface only after 2250.

As the pretornadic vorticity maximum intensified, a local region of increased westerly momentum developed to the south and east of the vorticity maximum (Figs. 9a and 9b), producing a bulge in the gust front. Although the bulge in the gust front was weakening/retreating at 2259, cyclonic shear and curvature were increasing near the gust front 3–4 km east and east-northeast of tornado 1 (Fig. 9c). The first step of cyclic vortexgenesis had begun; V2 marks the new region of weak vertical vorticity that would later be associated with tornado 2.

Vortex 2 was a much more prominent feature by the time of the next aircraft pass (Fig. 9d); the circulation was within 4 min of producing a visible condensation funnel. The new vortex was beginning to produce a new bulge in the gust front (Figs. 9d and 9e). Tornado 1 was beginning to turn to the left and become separated from the main rear gust front (Fig. 9d).

At 2313, the ropelike tornado 1 was within the trailing precipitation region (Figs. 9e and 5f). The resolved vorticity maximum in the dual-Doppler analysis is narrow and weak (Fig. 9e). Several kilometers to its northeast, the magnitude of vorticity had increased in the flow surrounding the incipient tornado 2. With a strong vortex and a nearby bulge in the rear gust front, the wind field in the tornadic region resembled that observed earlier (Figs. 9c and 9e). Cyclonic curvature in the flow (labeled V4) was increasing near the gust front east of tornado 2 (Fig. 9e). One may even trace the new feature back to the previous pass (near $x = -2.5$, $y = -9$ in Fig. 9d).

Earlier, the formative stage of V2 was characterized by increasing values of circulation with height (as indicated by a larger region with vertical vorticity greater than 0.02 s^{-1} at 4.0 km AGL than at 0.5 km in Figs. 9c and 11a). The new vorticity maximum V4 was especially more prominent aloft than at low levels (Figs. 9e and 11b). The increase in vorticity with height represents a minor departure from the Burgess et al. (1982) model, in which new vortices grow rather uniformly with height. As had also been the case earlier during the transition from tornado 1 to tornado 2 (Fig. 11a), the ~5 km scale mesocyclonic flow at 4 km AGL was subdivided into a concentrated vortex associated with the existing tornado and a broader developing vorticity maximum to its east (Fig. 11b).

Low-level rotation increased with time in the newest vortex (Figs. 9e–h), which later tightened into the large F4 tornado 4 (Figs. 3 and 4d). Although we have labeled the vorticity maximum V4 to associate it with tornado 4, it apparently also was associated with the brief tornado 3 (Figs. 3 and 4c). This tornado occurred while the Electra aircraft was turning around after the pass at 2318. There is no evidence of a tornado signature in reflectivity and radial velocity in the raw ELDORA data at 2318 and 2325. Therefore, we can say little about this tornado other than to note that visually it appeared to be a feature along the gust front southeast of the main center of rotation in the cloud base, and it was too small and/or short lived to be detected.

Like the first tornado, tornado 2 weakened, became separated from the main gust front, and dissipated within heavy precipitation along the rear flank (Figs. 9f and 9g). Since there is no evidence of reintensification of either posttornadic vorticity maximum, the analyses of the McLean storm are inconsistent with the Agee et al. (1976) model. The pattern of tornadogenesis resembles that in the Burgess et al. (1982) model (Fig. 1), in which new vorticity maxima form to the east of mature ones and dissipating vortices move northwestward. However, the resolved vorticity maxima in this case are smaller than those in the radar observations (4–6 km wide) examined by Burgess et al. The apparent difference in size may be partly related to the difference in ranges of the observations. The Burgess et al. dataset included targets up to 150 km from the radar.

The cyclic formation of large tornadoes ended with Tornado 4, the strongest and longest-lived tornado of the group (Fig. 3). As at earlier times, there was cyclonic vorticity >0.01 s^{-1} near the bow in the gust front to the northeast and east of the tornado (Figs. 9h and 9i). Although Tornado 5 (Fig. 4d) was apparently too small and/or weak to have a clear signature in the ELDORA data, it may have been associated with the secondary local maximum in vorticity near the gust front at 0003 (near $x = 12.5$, $y = 18$ in Fig. 9i). However, in general, the vorticity near the gust front during Tornado 4 tended to be distributed along an arc rather than in discrete, growing disturbances.

In the Burgess et al. (1982) model, the next mesocyclone in a series forms at an occlusion point between the wrapping rear-flank gust front and the gust front extending to the east along the forward flank (Fig. 1). In contrast, the pseudo-dual-Doppler analyses at 500 m AGL indicate a gradual turning of the winds, rather than a distinct wind shift, to the east of the rear-flank gust front in the regions where vortices 2 and 4 formed (Figs. 9c, 9e, 10a, and 10b). Although an elongated region of upward motion is indicated extending southeastward from near V2 at 2259 (Fig. 10a), this feature could be considered spurious since it was near the edge of the data-coverage region, and it was not present at the previous or the next time (not shown). Forward-flank wind shifts, when present at all, tended to be weak and generally extended to the north or northeast from the dominant vorticity maximum (e.g., Figs. 9a–c and 9e–g). Although the location of new vorticity maxima with respect to the rear-flank gust front is consistent with the Burgess et al. (1982) model, the lack of a strong low-level wind shift along the forward flank is more consistent with the results of numerical simulations (e.g.,

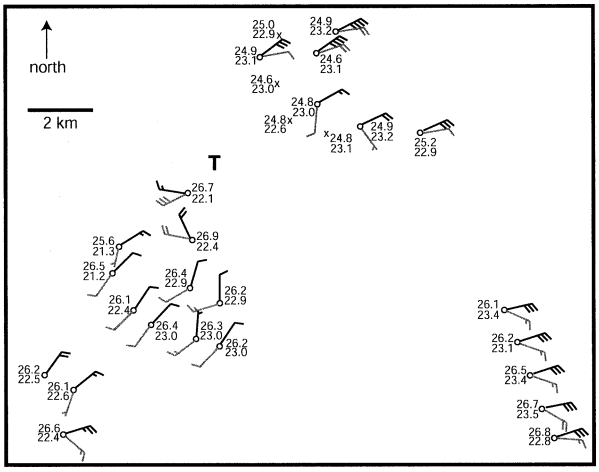

FIG. 12. Mobile-mesonet observations (courtesy of P. Markowski) at 0017 UTC 9 Jun 1995. Storm-relative (ground relative) winds are indicated in black (gray). Storm motion is (U = 7 m s^{-1}, V = 8 m s^{-1}). Full wind barbs represent 5 m s^{-1}. The positions of the mobile-mesonet observations are based on time-to-space conversion over a 5-min period. Temperature (upper number) and dewpoint (lower number) are in °C. The location of tornado 4 is labeled T.

Adlerman et al. 1999). In Part II of this paper, we will discuss the formation of new vorticity maxima in more detail.

In situ measurements near the surface are available during the mature stage of tornado 4 (Fig. 12). Wind speeds at 3 m AGL (approximately 10 m s^{-1}) were generally significantly less than at 500 m AGL (approximately 25 m s^{-1}) (Fig. 9). Compared to that in supercell simulations (e.g., Rotunno and Klemp 1985), the low-level temperature field at 0017 (Fig. 12) and later times was unusual. In particular, the air southwest of the tornado behind the rear-flank gust front was not cool, but instead was of approximately the same temperature as the inflow from the near environment (Fig. 12). Direct measurements in other cases since 1994 support previous observations (e.g., Rasmussen et al. 1982) that a lack of cold air in this region may be quite common for developing and mature supercell tornadoes (Markowski et al. 2000).

b. Updraft characteristics

1) BACKGROUND

Although the traditional model of a supercell involves a single updraft (Browning 1964), observational studies (e.g., Weaver and Nelson 1982) have established the existence of multiple updrafts in some storms with supercell characteristics. Analyses of radar observations of supercells have included efforts to classify the propagation of the storm (i.e., the motion of the storm relative to the mean wind) as either continuous or discrete (Marwitz 1972; Lemon 1976; Weaver and Nelson 1982). In the former case, the mature stage of the storm is characterized by a long-lived quasi-steady main updraft. In the latter case, the storm (i.e., the persistent, organized process that produces severe weather) is maintained by a series of relatively short-lived updrafts.

Previous conceptual models of cyclic low-level vortex formation in supercells involve discrete propagation of the main updraft (Lemon and Doswell 1979; Klemp 1987; Adlerman et al. 1999). In these models, strong low-level rotation wraps cold outflow around the updraft, cutting off the updraft from potentially buoyant low-level air. This leads to the demise of the main updraft and, eventually, the vortex associated with it. However, the storm may persist if outflow from the mature cell initiates the formation of a new updraft nearby. If conditions remain favorable for the formation of low-level rotation within successive updrafts, then a family of vortices may be produced.

Complexities in storm structure can make it difficult to classify storm propagation as either continuous or discrete. Since finescale observations tend to reveal finescale features, the classification may be affected by the resolution of the observations (Battan 1980; Adlerman and Droegemeier 2000). Furthermore, the characteristics of the updraft may differ over the depth of the storm (Nelson and Braham 1975; Adlerman et al. 1999). Purely continuous or discrete propagation may be extremes within a spectrum of storm behaviors evaluated in terms of updraft structure and steadiness.

Since we are primarily interested in low- and midlevel processes in tornadogenesis studies, we will focus on the characteristics of the updraft within several kilometers of the ground. In the numerical simulation of a cyclic storm by Adlerman et al. (1999), the gust front surge associated with the intensifying low-level rotation initiated downshear updraft development. The contiguous midlevel updraft region contained two local vertical velocity maxima of approximately the same magnitude and size; one maximum was associated with the initial updraft, and the other was associated with the new downshear development. After examining the results of additional simulations, Adlerman and Droegemeier (2000) noted that the apparent midlevel updraft characteristics depended on the distance between the low-level mesocyclone and the bow in the rear gust front. When the separation was large, two distinct updraft centers developed with downdraft in between. For small separation, the updraft appeared more continuous, although it contained two inner maxima during the period of low-level occlusion.

2) OBSERVATIONS OF THE MCLEAN STORM

The vertical-velocity fields in the McLean storm were rather unsteady during the tornadic stage, and the analyses indicate multiple significant updrafts (Fig. 10). We have identified the ''main updraft'' (labeled with the letter M in Fig. 10) as the vertical velocity maximum that was typically closest to the tornadoes, greatest in magnitude, and largest in horizontal extent. Throughout

the cyclic stage of the storm, other updrafts formed and dissipated near the main updraft. Perhaps the most significant of these were the trailing updrafts that formed to the southwest of the main updraft after 2300 (Fig. 10b). With time, the trailing updrafts consolidated into a miniature line that merged into the south side of the main updraft (Figs. 10b–e). Afterward, during the life of tornado 4, the main updraft aloft again became rounder and more isolated (Fig. 10f).

Tornadoes tended to be located southwest or west of the main updraft maximum (Figs. 10a, 10b, and 10f), while new vorticity maxima tended to form along the east side of the updraft (Figs. 10a and 10b). When new vortices were forming, a conspicuous second updraft center (Adlerman et al. 1999) did not develop within the updraft region aloft (Figs. 10a and 10b). The observed updraft evolution is more consistent with that in simulations (Adlerman and Droegemeier 2000) in which the gust front does not surge far ahead of the existing tornado and main updraft.

For the temporal and spatial scales resolved in the wind syntheses, the main updraft appeared be a continuous feature during the tornadic stage. Some of the analyses do, however, indicate secondary updraft maxima (labeled with the letter S in Figs. 10b–d) near the tornadoes. We favor an interpretation of ''shedding'' (Adlerman and Droegemeier 2000) or ''separation'' of the vortex and a portion of the updraft from the main updraft. The updraft portion that is shed is considerably smaller than the original main updraft region. For example, the analysis indicates a small vertical velocity maximum just north of tornado 2 (S in Fig. 10c and at 0.5 km AGL in Fig. 10d) during the period when the distance of tornado 2 from the center of the main updraft was increasing. Earlier, the weakening tornado 1 was also associated with an updraft maximum that was smaller and weaker than the main updraft (Fig. 10b), but the interpretation is complicated by the general unsteadiness of the vertical velocity field to the southwest of the main updraft. In contrast to what is implied in previous conceptual models of the cyclic formation of vortices in supercells (Lemon and Doswell 1979; Klemp 1987), the formation of outflow around a strong vortex did not appear to isolate most of the main updraft from low-level air from the environment. Throughout the tornadic stage, low-level outflow did not surge ahead of the location of the updraft aloft. If the surface measurements of temperature behind the gust front at 0017 (Fig. 12) are representative of earlier times, then the air that was wrapped beneath the updraft by the low-level circulations was not cold.

c. *Modified conceptual model*

Our schematic of low-level evolution in a cyclic storm (Fig. 13) is reminiscent of the original diagram by Burgess et al. (1982, Fig. 1). We have added a depiction of low-level updrafts and downdrafts and have also included a few minor modifications motivated by this case study. A subtle difference in our diagram is that the two tornadoes move to the left relative to the storm track for the entire time, rather than just at the end, for reasons to be discussed in Part II.

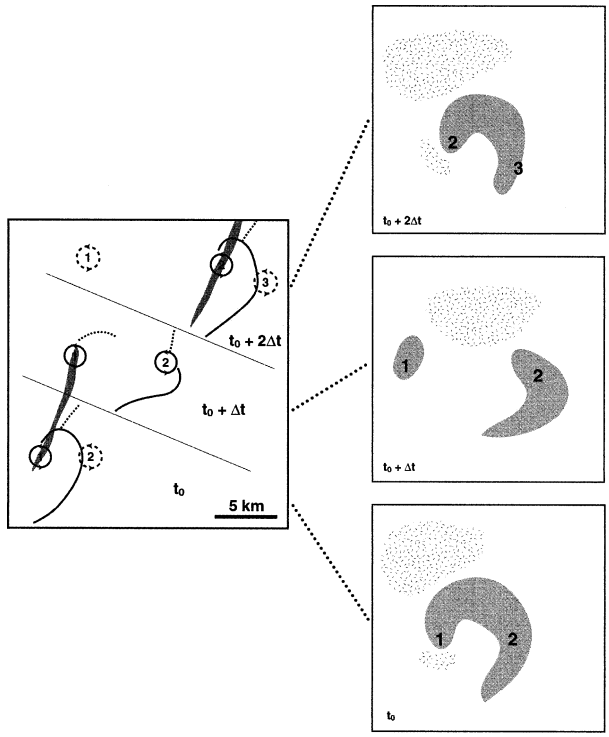

FIG. 13. Schematic at low levels of cyclic supercell tornadogenesis. (left) Circles and thick lines indicate vortices and wind shifts, respectively. Tornado tracks are shaded. (right) Shading indicates updraft, and the spotted pattern indicates downdraft. The time between successive tornadoes ($2\Delta t$) is ~20 min.

A new vorticity maximum forms near the rear-flank gust front, ahead and to the right (i.e., to the east in this case of a northeastward moving storm) of the tornado (time t_0 in Fig. 13). At this stage, the vorticity in the new local maximum increases in magnitude with height. The vorticity maximum does not necessarily form at an occlusion point between rear-flank and forward-flank gust fronts. Wind shifts along the forward flank, when present, may be very weak. Furthermore, the low-level ''gust fronts'' may be purely kinematic features that are not supported by a low-level cold pool.

The existing tornado loses its connection with the main gust front, and a small portion of updraft separates from the main updraft (time $t_0 + \Delta t$ in Fig. 13). Both the tornado and small updraft region move rearward relative to the storm-scale updraft and eventually dissipate. Meanwhile, the new low-level vorticity maximum strengthens, and it begins to control the movement of the gust front. Air sweeps around the right side of the vorticity maximum, producing a new bulge in the gust front.

By the time the new vortex has reached tornadic in-

tensity (time $t_0 + 2\Delta t$ in Fig. 13), yet another vorticity maximum has begun to form near the new bow-shaped portion of the gust front. Vorticity typically decreases with height from low levels to midlevels in the vorticity maximum associated with the tornado but increases with height in the newest vorticity maximum. The evolution of the vorticity profiles in the McLean storm will be discussed in more detail in Part II.

One complete cycle is included in Fig. 13; several cycles may occur in some storms. The time between successive tornadoes ($2\Delta t$) was less than 20 min in the McLean storm (Fig. 3). This time is relatively fast compared to that in some numerical simulations of cyclic storms (Adlerman et al. 1999) but is not unusual (e.g., Jensen et al. 1983).

5. Conclusions

The pseudo-dual-Doppler syntheses of the ELDORA data from 8 June 1995 are sufficient for depicting relationships among the tornadoes, rear-flank gust front, and parent updraft every 5–6 min. The relative locations of the tornadoes and the rear-flank gust front in the McLean storm were consistent with those in traditional conceptual models of tornadic supercells (Lemon and Doswell 1979; Burgess et al. 1982; Adlerman et al. 1999). The tornadoes themselves are not resolved in the wind fields synthesized from the dual-Doppler data, but the three largest tornadoes in the McLean storm are associated with prominent vorticity maxima in the synthesized wind fields. New vorticity maxima formed near bulges in the rear-flank gust front to the east of existing tornadoes.

Since the time interval (5–6 min) between aircraft passes is relatively long, uncertainty is introduced into the interpretation of storm evolution. Even though the main updraft in the McLean storm had an unsteady shape initially and was often flanked by other updrafts to its southwest and west, there is a single identifiable main updraft at each analysis time after 2242. To the degree to which the time sampling permits assessment, the main updraft appeared to be a continuous feature. In contrast, dissipation of a substantial portion of the main updraft, and reformation of a new main updraft elsewhere, are elements of previous conceptual models of supercells during the transition stage between successive tornadoes (Lemon and Doswell 1979; Klemp 1987). In the McLean storm, a tornado, once formed, was able to persist up to several kilometers away from the parent updraft (e.g., Fig. 10b). In the cases of both tornado 1 and 2, a small portion of the updraft separated from the main updraft when the tornado moved rearward.

In the simulation by Adlerman et al. (1999), the rear-flank gust front, which was supported by a strong low-level cold pool, moved several kilometers ahead of the original updraft aloft. The new downshear updraft at midlevels, which had its roots along the rear-flank gust front, was initially tilted. The formation of the next low-level vortex in the series did not occur until the low-level outflow weakened, and the new updraft became more erect. In contrast, the rear-flank gust front in the McLean storm did not move beyond the updraft aloft, and, at least during the mature stage of tornado 4, there was no relatively cold air behind it. When outflow is weak and the gust front remains beneath the updraft aloft, a storm may be able to produce tornadoes relatively frequently since there is no intermediate time required for the updraft to re-form and reorganize.

A number of questions arise from the qualitative presentation thus far: What was the source of vertical vorticity in the tornadoes? Why did the cyclic formation of large tornadoes end with tornado 4? Questions such as these will be addressed in Part II of this study.

Although we are hesitant to make general conclusions from only one case, the type of storm observed on 8 June 1995 near McLean, Texas, nevertheless may be common during tornado outbreaks. We await high-resolution measurements in other cyclic storms for comparison. An informal survey of other cases revealed more examples of intense, long-lived tornadoes that were preceded by a series of shorter-lived tornadoes. For example, the storm that produced a long-lived tornado with F5 damage in Oklahoma City on 3 May 1999 had earlier produced eight shorter-lived tornadoes (Speheger et al. 2002). For future work, we propose compiling a more detailed climatology of cases with long-lived tornadoes (i.e., cases with tornadoes that last ~1 h). The climatology could be used to address the following questions: What fraction of long-lived tornadoes are preceded by a series of short-lived tornadoes? Are the environmental conditions of storms with long-lived tornadoes similar? The sensitivity of low-level vortex longevity to the environmental conditions could be explored with a series of numerical simulation experiments.

Acknowledgments. This work was funded by National Science Foundation Grants ATM-9612674 and ATM-991209, and was completed while the lead author was supported by the Cooperative Institute for Mesoscale Meteorological Studies (NSF Grant ATM-000412). We thank all VORTEX participants for their contributions. In particular we acknowledge Erik Rasmussen for leading the field project, Roger Wakimoto for directing the Electra aircraft operations, the NOAA P-3 and NCAR Electra flight crews for making the collection of airborne Doppler data possible, and Jerry Straka for helping design and coordinate the mobile mesonet operations.

Wen-Chau Lee provided the ELDORA data and answered many questions about data processing. Michelle Case and Dick Oye assisted with the REORDER objective analysis software. The Grid2ps software by Susan Stringer and Wen-Chau Lee was an essential tool in the development of graphics for this paper. David Ewoldt, Bruce Haynie, Cristina Kaufman, Tim Mar-

shall, Scott Richardson, and Herb Stein provided video and photographic documentation of the McLean storm. Doug Crowley supplied information on the surveys of the McLean tornadoes by the Amarillo, Texas, National Weather Service office. We appreciate the input of the following individuals on various aspects of this work: Chuck Doswell, Matt Gilmore, Mike Magsig, Morris Weisman, and Lou Wicker. In addition, the comments of three anonymous reviewers were quite helpful. This research would not have been possible without the computer assistance of Tom Condo and Mark Laufersweiler at the University of Oklahoma.

APPENDIX

Pseudo-Dual-Doppler Wind Synthesis

a. Preprocessing of data

Before synthesizing the pseudo-dual-Doppler wind, we edited the raw ELDORA radar data with the SOLO (Nettleton et al. 1993; Oye et al. 1995) software package developed at NCAR. SOLO removes the aircraft motion component from the radial velocities (Lee et al. 1994) during data conversion and then allows the user to ''edit'' the data. Editing involves unfolding aliased radial velocities and removing reflectivity and velocity data that are not representative of the storm and its environment (e.g., data contaminated as a result of ground clutter and range folding). Since the effective Nyquist velocity interval is so large (nearly ± 80 m s^{-1}) with dual pulse repetition frequency (PRF) scanning by the ELDORA, velocities were folded in only a few locations. A disadvantage of the dual-PRF technique is that it results in velocity ''speckles.'' If the velocity estimate associated with either of the PRFs is in error by a few meters per second, then the categorization algorithm associates these measurements with a velocity much different from the true velocity (Sirmans et al. 1976). Since only a small fraction of the velocity estimates were speckled (fewer than 5%), we opted to remove them rather than to attempt to correct them subjectively. We did not remove all the speckles in the turbulent region above 10 km AGL in and near the top of the updraft, except in the data from one aircraft pass. Since a comparison of two dual-Doppler wind syntheses of these data, one with and the other without the upper-level speckles deleted, revealed negligible differences in the derived vertical velocities below 6 km, we did not attempt to remove all the upper-level speckles from the other data.

b. Interpolation of data

The resolution of the ELDORA data depends on the along-track data spacing ($\sim$300 m) and the beamwidth (310–470 m for typical ranges of 10–15 km to the McLean storm updraft and tornadoes). If we assume that the maximum sampling dimension is 470 m and that a minimum of six independent points is necessary to resolve a feature (Carbone et al. 1985), then it follows that features narrower than 2800 m will be poorly resolved. We selected horizontal and vertical grid spacings of 400 and 500 m, respectively, for the interpolation of raw data to Cartesian grids. The radius of influence for the Cressman (1959) weighting scheme in the REORDER software (Oye et al. 1995) was 800 m.

c. Reference frame

One of the assumptions inherent in traditional dual-Doppler analysis is stationarity of the wind field. For nonsimultaneous observations, Gal-Chen (1982) showed that this condition is violated the least when the Doppler wind data are analyzed in a moving reference frame in which the storm is most steady. Gal-Chen's variational method for determining the motion of the optimal reference frame is formulated for radars at fixed sites. Since airborne radars do not scan from fixed locations, we defined the variational problem in terms of the Cartesian wind components rather than the radial velocities (Gal-Chen 1982), as follows:

$$J_s(U_s, V_s) = \int_{R^{(4)}} \left[\left(\frac{\partial u'}{\partial t'}\right)^2 + \left(\frac{\partial v'}{\partial t'}\right)^2 + \left(\frac{\partial w'}{\partial t'}\right)^2 \right] dR^{(4)} = \text{minimum}, \quad \text{(A.1)}$$

where (U_s, V_s) is the optimal horizontal storm translation velocity for the wind synthesis, $R^{(4)}$ is a bounded region in time and space, and primes refer to quantities in the moving frame (e.g., $\partial u'/\partial t' = \partial u/\partial t + U_s \partial u/\partial x + V_s \partial u/\partial y$). The solution of (A.1) is complicated by the dependence of the Cartesian wind components (from the dual-Doppler wind synthesis) on U_s and V_s. We used an iterative approach (Gal-Chen 1982; Matejka 2002) with the following steps to determine U_s and V_s and synthesize the wind field:

1) Interpolate the raw observations to a Cartesian grid with REORDER.
2) Synthesize the Cartesian wind components u, v, and w with the procedure described below.
3) If the specified number of iterations has been executed, then end the procedure. Otherwise, solve the variational problem (A.1) for U_s and V_s (Gal-Chen 1982).
4) Adjust the locations of the observations (i.e., the gridded observations from step 1) according to the new estimates of U_s and V_s. Then, interpolate these irregularly spaced observations back to a regular grid.
5) Repeat the procedure beginning at step 2.

For the analyses of the ELDORA data of the McLean storm, we determined (U_s, V_s) for the center volume in each set of three consecutive dual-Doppler volumes. The

initial interpolation of the raw data to Cartesian grids (step 1) included a correction for translation, but the values of U_s and V_s had to be prespecified as input to the REORDER software. We estimated the motion (U, V) (Figs. 9 and 10) of the dominant low-level vortex during each aircraft pass and provided these values, which represent a first guess of (U_s, V_s), as input to REORDER. Then, we executed the iterative procedure described above to refine the estimates of (U_s, V_s). We attempted to incorporate the entire reference-frame algorithm directly into the REORDER objective analysis software but were unsuccessful. Therefore, the wind synthesis procedure involved two Cressman interpolations (steps 1 and 4); the second interpolation was in the horizontal only. The application of two Cressman interpolations with a larger radius of influence (800 m) than the mean data spacing (400 m) resulted in relatively smooth wind fields. For example, the amplitudes of features with wavelengths of $4\Delta x$ (1600 m) were damped by approximately 50% by each Cressman interpolation (Trapp and Doswell 2000). No other explicit filtering was used in the wind synthesis procedure.

Gal-Chen (1982) described a solution of (A.1) when $R^{(4)}$ encompasses the entire moving domain. During the analysis of the ELDORA data, we experimented with a method that allows (U_s, V_s) to vary in space (Dowell and Bluestein 1999). The motivation for this approach was that the motion of individual features changed with time, and different features within the domain moved at different characteristic velocities. For example, although the mean storm motion was toward the northeast, tornado 1 turned toward the northwest (Fig. 3). Tornado 2 also moved northwest, although the trailing gust front was advancing eastward in a storm-relative sense (Fig. 9).

For the analyses presented in this paper, we computed local reference frame motions by solving (A.1) within 3-km-wide cubes centered around each grid point during each of five iterations of the overall procedure. The choices of the parameters were based on tests of the procedure on numerically simulated airborne radar data. For simulated observations of both colliding low-level cold pools and thunderstorms (including supercell and multicell storms) (Dowell and Bluestein 1999), the best results were obtained when the local subdomains were 5–10 times as wide as the grid spacing (i.e., comparable in size to the smallest resolvable scale). Furthermore, three to six iterations of the procedure for estimating the reference-frame motion and synthesizing the wind field produced the most accurate results. Additional iterations either provided no additional benefit or resulted in eventual divergence of the solution. Convergence of the iterative procedure is guaranteed neither for the case of the uniform nor the nonuniform reference frame, especially for typical airborne scanning geometry (Matejka 2002). In all tests, including those both with and without noise added to the simulated observations, the use of a nonuniform reference frame over a uniform moving reference frame resulted in minor improvement of the synthesized wind fields. The magnitude of the decrease in the rms errors of the synthesized velocities ranged from 5% to 13% and depended on the magnitudes of the radial velocity errors, the locations of the radars, the time lags between fore and aft scans, the times required to collect entire volumes, and the characteristics of the simulated phenomena.

For the ELDORA data centered at 2313, the procedure for determining the motion of the reference frame converged on values of ($U_s = 3$ m s^{-1}, $V_s = 8$ m s^{-1}) when the translation velocity was required to be uniform within the domain (Fig. A1a). These values are representative of overall storm motion. When the translation velocity was non-uniform, the results indicated more appropriate motion toward the northwest in the vicinity of tornadoes 1 and 2 (Fig. A1b). Despite the differences in the moving reference frames, the differences in the synthesized vertical velocities are relatively minor and would probably not affect qualitative interpretation of the analyses. If the reference-frame algorithms could be applied directly to the raw data, rather than previously gridded data as in step 4, then the differences between the two results could be more significant.

The Euler–Lagrange equations of (A.1) are a set of two equations and two unknowns (U_s and V_s) (Gal-Chen 1982). The coefficients of the unknown variables in these equations are integrals over space and time of the spatial derivatives of the Cartesian wind components. A region with weak gradients requires special treatment because the determinant of the coefficient matrix is relatively small there. We have implemented a procedure that forces the solution toward ($U_s = 0$, $V_s = 0$) when the determinant of the system approaches zero.

Our work with the use of nonuniform moving reference frames is preliminary. In future experiments with this technique, we would prefer to avoid two interpolations (steps 1 and 4 in the algorithm) by incorporating the reference-frame algorithm directly into software that interpolates raw ELDORA data to a grid. Sensitivity to the first guess (U, V) could be avoided, and the maximum possible improvement in the results could potentially be obtained. In addition, a new formulation of the cost function by Matejka (2002) may lead to more robust procedures for determining U_s and V_s.

d. Wind synthesis

1) SOLUTION OF THE VARIATIONAL FORMULATION

For the wind synthesis, we used a variational method with weak constraints like that proposed originally by Gamache (1997). The solution for the three unknown velocity components [$u(x, y, z)$, $v(x, y, z)$, $w(x, y, z)$] is that which yields a minimum in the following functional:

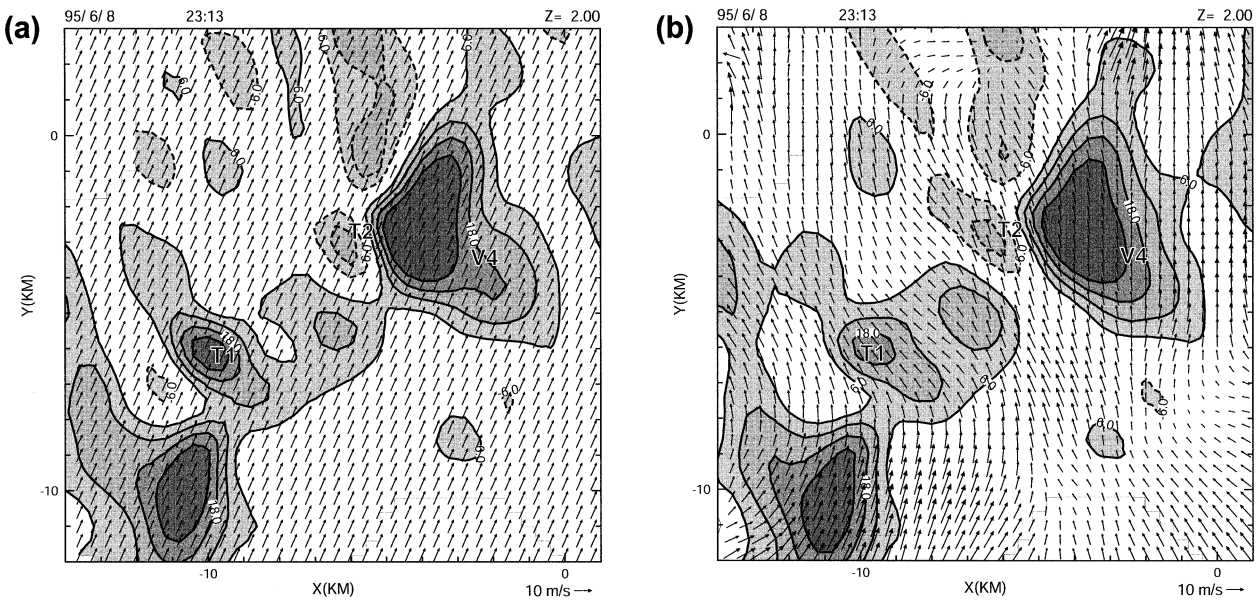

FIG. A1. Horizontal translation velocity (U_s, V_s) of moving reference frame (vectors) and vertical velocity (shading and contours; negative values are contoured with dashed lines) at 2.0 km AGL at 2313 UTC. The contour interval for vertical velocity is 6.0 m s^{-1}. Other labels are as in Fig. 9: (a) uniform translation velocity (U_s = 3 m s^{-1}, V_s = 8 m s^{-1}) and (b) nonuniform translation velocity.

$$J_d = \iiint_{R^{(3)}} \Big\{ [c_1^{(1)}u + c_2^{(1)}v + c_3^{(1)}(w + w_t) - v_r^{(1)}]^2 + [c_1^{(2)}u + c_2^{(2)}v + c_3^{(2)}(w + w_t) - v_r^{(2)}]^2 + \beta\left(\frac{\partial u}{\partial x} + \frac{\partial v}{\partial y} + \frac{\partial w}{\partial z} - \kappa w\right)^2 \Big\}\, dx\, dy\, dz = \text{minimum}, \quad \text{(A.2)}$$

where β is a prespecified weight, $\kappa = -\partial(\ln\overline{\rho})/\partial z$, $\overline{\rho}(z)$ is the base-state density, $R^{(3)}$ is a bounded 3D region, v_r denotes a radial velocity measurement, and the superscripts identify the radar number. (In this case, 1 and 2 refer to the fore and aft radars, respectively.) The wind field thus satisfies both the observations and the anelastic mass continuity equation in a least squares sense over the domain. Our experiments with numerically simulated radar data indicate than when significant random errors (~1 m s^{-1}) are present in the measurements, the solution to (A.2) is more accurate than that from traditional methods (e.g., Armijo 1969; Brandes 1977), in which the observations are satisfied exactly. In addition, there is no restriction on radar elevation angles (Gamache 1997) in the solution of (A.2) as in other traditional Cartesian methods (Ray et al. 1985).

The c coefficients in Eq. (A.2), which relate the Cartesian wind components to the projection of the velocity in the direction of the radar beam, are given below in earth-relative coordinates:

$$c_1 = \sin a \cos e, \quad \text{(A.3)}$$

$$c_2 = \cos a \cos e, \quad \text{and} \quad \text{(A.4)}$$

$$c_3 = \sin e, \quad \text{(A.5)}$$

where a is the azimuth angle (measured clockwise from due north) and e is the elevation angle (measured upward from horizontal). To estimate the precipitation fall speed w_t, we used an empirical relationship based on the reflectivity factor:

$$w_t = \begin{cases} \left(\dfrac{\rho_0}{\overline{\rho}}\right)^{0.4} (0.70 - 0.35 Z_{\mathrm{dB}}), & \text{if } Z_{\mathrm{dB}} > 2\ \mathrm{dB}Z_e \\ 0, & \text{otherwise,} \end{cases} \quad \text{(A.6)}$$

where Z_{dB} is the reflectivity factor in dBZ_e, w_t is in meters per second, and the values are adjusted for the base-state air density (Foote and duToit 1969). We developed the empirical relationship (A.6) specifically for the 8 June 1995 ELDORA data by investigating radial velocity measurements in precipitation directly above the flight track. Since these data were collected in a variety of locations away from the major updraft and downdraft regions of the storm, we assumed that the mean vertical *air* velocity of the samples was zero when fitting equation (A.6) to the data. If a storm is steady between the times of the fore and aft samples, then the dual-Doppler measurements above the flight track provide a direct estimate of the scatterer vertical velocity. For the observed values of reflectivity, the values of w_t from (A.6) are up to 80% larger than those from the Joss and Waldvogel (1970) empirical equation. This may indicate that the measurements in the regions of high reflectivity in the McLean storm were dominated more by large drops and/or hail relative to the measurements in the storms considered by Joss and Waldvogel.

A number of options were available for the solution

of (A.2). Gamache (1997) and Gao et al. (1999) used conjugate gradient methods to obtain values of the wind components that produced a minimum in the cost function. Shapiro and Mewes (1999) obtained a direct solution by expressing the Euler–Lagrange equations of (A.2) in a cylindrical (coplane) coordinate system. For convenience, we chose instead to work in Cartesian coordinates. We derived the three Euler–Lagrange equations associated with (A.2) by taking the variation of J_d with respect to each Cartesian wind component and requiring each variation to be zero. Although the three equations are coupled in the unknowns u, v, and w, we were able to obtain solutions by iteration. A drawback of the iterative approach is that it is possible for the winds to converge on a local minimum, rather than on the global minimum, in the cost function (Shapiro and Mewes 1999). For the datasets in this study, we found that the final solution was rather insensitive to the first guess. We initialized the iterative procedures by projecting the coplanar dual-Doppler velocity onto the Cartesian components at each grid point. Inherent in this method is the initial guess that the velocity component normal to the common plane of the observations is zero.

We are unaware of a quantitative method for determining the optimum weight β in (A.2) for a dataset with unknown measurement errors. To provide guidance in the choice of β, we tested the wind synthesis method on numerically simulated radar data (Dowell and Bluestein 1999) with random radial velocity measurement errors having a standard deviation of 1–2 m s^{-1}. Based on this test, we chose $\sqrt{\beta} = 500$ m for the pseudo-dual-Doppler analyses discussed in this paper. The solution of the variational problem (A.2) satisfies the observations approximately rather than exactly. For the given choice of β, the mean value of $|c_1u + c_2v + c_3(w + w_t) - v_r|$ for the analyses of the McLean storm was 0.5 m s^{-1}.

2) Boundary conditions

In the derivation of the Euler–Lagrange equations, we used the following boundary conditions: 1) $w = 0$ at both the surface and the top of the storm, and 2) continuity is satisfied *exactly* at the lateral boundaries of the domain. In most of the grid columns, we defined the top of the storm as 12 km AGL (the mean height of the McLean storm's anvil). However, in columns where the high-reflectivity region extended above 12 km (e.g., in overshooting thunderstorm tops), we defined the top of the storm as the highest level where the reflectivity factor exceeded 20 dBZ. Errors in the upper boundary condition for w are likely significant (~10 m s^{-1}). However, we believe it is preferable to incorporate this physical constraint into the synthesis (even with its anticipated error) in order to eliminate the larger problems with w associated with accumulation of errors in the divergence estimates.

Since radar data near the surface that were contaminated by ground clutter were deleted during the editing step, the lower boundary condition was problematic as well. The height of the lowest uncontaminated data varies with range but is approximately 500 m AGL for the more distant (range ~15 km) observations of the tornadoes. For the dual-Doppler wind syntheses, we assumed that the horizontal divergence estimate at z = 500 m was representative of the layer below. Since the magnitude of convergence is not necessarily uniform with height in the boundary layer in and near a supercell (Dowell and Bluestein 1997), the lack of measurements near the surface presents a real challenge in synthesizing low-level vertical velocities. This source of error is likely to be especially significant near tornadoes, which tend to have very shallow low-level inflow (Lewellen 1993; Wurman et al. 1996).

3) Centrifuging effects

Tornadoes in the McLean storm and in other supercells observed by the ELDORA during VORTEX (Wakimoto et al. 1996) were associated with weak-echo holes in reflectivity (Fig. 8). The observed reflectivity patterns probably resulted from centrifuging of scatterers by the tornadoes (Dowell et al. 2001). The discrepancy between the air motion and the motion of centrifuged precipitation and/or debris is a source of error in the wind synthesis. The magnitude of the error associated with centrifuging is a function of the intensity of the vortex, the characteristics of the targets producing backscattered radiation, and the sampling characteristics of the radar beam (Dowell et al. 2001). If the dominant scatterers were large (1 mm) drops of rain, then the estimates of divergence in the resolved vortices in this case may have been 0.002–0.01 s^{-1} too high. Without knowing the characteristics of the distribution of scatterers, we are unable to correct for this error.

4) Hole-filling procedure

Dual-Doppler observations do not completely fill the analysis domains. To keep the wind synthesis simple, we filled the holes in the data with velocity components that satisfied the centered finite-difference forms of the 2-D Laplace equations:

$$\frac{\partial^2 u}{\partial x^2} + \frac{\partial^2 u}{\partial y^2} = 0, \qquad \frac{\partial^2 v}{\partial x^2} + \frac{\partial^2 v}{\partial y^2} = 0,$$

$$\frac{\partial^2 w}{\partial x^2} + \frac{\partial^2 w}{\partial y^2} = 0. \tag{A.7}$$

This method of filling minimizes the introduction of horizontal divergence in the data voids (Ellis 1997). After completing the variational dual-Doppler synthesis, we discarded these values that were created artificially.

REFERENCES

Adlerman, E. J., and K. K. Droegemeier, 2000: A numerical simulation of cyclic tornadogenesis. Preprints, *20th Conf. on Severe Local Storms*, Orlando, FL, Amer. Meteor. Soc., 591–594.

——, ——, and R. Davies-Jones, 1999: A numerical simulation of cyclic mesocyclogenesis. *J. Atmos. Sci.,* **56,** 2045–2069.

Agee, E. M., J. T. Snow, and P. R. Clare, 1976: Multiple vortex features in the tornado cyclone and the occurrence of tornado families. *Mon. Wea. Rev.,* **104,** 552–563.

Armijo, L., 1969: A theory for the determination of wind and precipitation velocities with Doppler radars. *J. Atmos. Sci.,* **26,** 570–573.

Battan, L. J., 1980: Observations of two Colorado thunderstorms by means of a zenith-pointing Doppler radar. *J. Appl. Meteor.,* **19,** 580–592.

Bluestein, H. B., E. W. McCaul Jr., G. P. Byrd, and G. R. Woodall, 1988: Mobile sounding observations of a tornadic storm near the dryline: The Canadian, Texas storm of 7 May 1986. *Mon. Wea. Rev.,* **116,** 1790–1804.

Brandes, E. A., 1977: Flow in severe thunderstorms observed by dual-Doppler radar. *Mon. Wea. Rev.,* **105,** 113–120.

Browning, K. A., 1964: Airflow and precipitation trajectories within severe local storms which travel to the right of the winds. *J. Atmos. Sci.,* **21,** 634–639.

Burgess, D. W., L. R. Lemon, and R. A. Brown, 1975: Tornado characteristics revealed by Doppler radar. *Geophys. Res. Lett.,* **2,** 183–184.

——, V. T. Wood, and R. A. Brown, 1982: Mesocyclone evolution statistics. Preprints, *12th Conf. on Severe Local Storms,* San Antonio, TX, Amer. Meteor. Soc., 422–424.

Carbone, R. E., M. J. Carpenter, and C. D. Burghart, 1985: Doppler radar sampling limitations in convective storms. *J. Atmos. Oceanic Technol.,* **2,** 357–361.

Cressman, G. P., 1959: An operational objective analysis system. *Mon. Wea. Rev.,* **87,** 367–374.

Darkow, G. L., 1971: Periodic tornado production by long-lived parent thunderstorms. Preprints, *Seventh Conf. on Severe Local Storms,* Kansas City, MO, Amer. Meteor. Soc., 214–217.

——, and J. C. Roos, 1970: Multiple tornado producing thunderstorms and their apparent cyclic variations in intensity. Preprints, *14th Conf. on Radar Meteorology,* Tucson, AZ, Amer. Meteor. Soc., 305–308.

Davies, J. M., C. A. Doswell III, D. W. Burgess, and J. F. Weaver, 1994: Some noteworthy aspects of the Hesston, Kansas, tornado family of 13 March 1990. *Bull. Amer. Meteor. Soc.,* **75,** 1007–1017.

Doviak, R. J., P. S. Ray, R. G. Strauch, and L. J. Miller, 1976: Error estimation in wind fields derived from dual-Doppler radar measurement. *J. Appl. Meteor.,* **15,** 868–878.

Dowell, D. C., and H. B. Bluestein, 1997: The Arcadia, Oklahoma, storm of 17 May 1981: Analysis of a supercell during tornadogenesis. *Mon. Wea. Rev.,* **125,** 2562–2582.

——, and ——, 1999: Dual-Doppler analysis of non-simultaneous observations. Preprints, *29th Conf. on Radar Meteorology,* Montreal, QC, Canada, Amer. Meteor. Soc., 529–532.

——, and ——, 2002: The 8 June 1995 McLean, Texas, storm. Part II: Cyclic tornado formation, maintenance, and dissipation. *Mon. Wea. Rev.,* **130,** 2649–2670.

——, ——, and D. P. Jorgensen, 1997: Airborne Doppler radar analysis of supercells during COPS-91. *Mon. Wea. Rev.,* **125,** 365–383.

——, J. Wurman, and L. J. Wicker, 2001: Centrifuging of scatterers in tornadoes. Preprints, *30th Conf. on Radar Meteorology,* Munich, Germany, Amer. Meteor. Soc., 307–309.

Ellis, S., 1997: Hole-filling data voids in meteorological fields. M.S. thesis, School of Meteorology, University of Oklahoma, 198 pp. [Available from School of Meteorology, 100 East Boyd, Norman, OK 73019.]

Foote, G. B., and P. S. duToit, 1969: Terminal velocity of raindrops aloft. *J. Appl. Meteor.,* **8,** 249–253.

Forbes, G. S., 1981: On the reliability of hook echoes as tornado indicators. *Mon. Wea. Rev.,* **109,** 1457–1466.

Fujita, T. T., 1974: Jumbo tornado outbreak of 3 April 1974. *Weatherwise,* **27** (3), 116–126.

——, 1981: Tornadoes and downbursts in the context of generalized planetary scales. *J. Atmos. Sci.,* **38,** 1511–1534.

——, D. L. Bradbury, and C. F. van Thullenar, 1970: Palm Sunday tornadoes of April 11, 1965. *Mon. Wea. Rev.,* **98,** 29–69.

Gal-Chen, T., 1982: Errors in fixed and moving frame of references: Applications for conventional and Doppler radar analysis. *J. Atmos. Sci.,* **39,** 2279–2300.

Gamache, J. F., 1997: Evaluation of a fully three-dimensional variational Doppler analysis technique. Preprints, *28th Conf. on Radar Meteorology,* Austin, TX, Amer. Meteor. Soc., 422–423.

Gao, J., M. Xue, A. Shapiro, and K. K. Droegemeier, 1999: A variational method for the analysis of three-dimensional wind fields from two Doppler radars. *Mon. Wea. Rev.,* **127,** 2128–2142.

Glickman, T. S., Ed.,2000: *Glossary of Meteorology.* 2d ed. Amer. Meteor. Soc., 855 pp.

Hildebrand, P. H., and C. K. Mueller, 1985: Evaluation of meteorological airborne Doppler radar. Part I: Dual-Doppler analyses of air motions. *J. Atmos. Oceanic Technol.,* **2,** 362–380.

——, C. A. Walther, C. L. Frush, J. Testud, and F. Baudin, 1994: The ELDORA/ASTRAIA airborne Doppler weather radar: Goals, design, and first field tests. *Proc. IEEE,* **82,** 1873–1890.

Jensen, B., E. N. Rasmussen, T. P. Marshall, and M. A. Mabey, 1983: Storm scale structure of the Pampa storm. Preprints, *13th Conf. on Severe Local Storms,* Tulsa, OK, Amer. Meteor. Soc., 85–88.

Johnson, K. W., P. S. Ray, B. C. Johnson, and R. P. Davies-Jones, 1987: Observations related to the rotational dynamics of the 20 May 1977 tornadic storms. *Mon. Wea. Rev.,* **115,** 2463–2478.

Jorgensen, D. P., P. H. Hildebrand, and C. L. Frush, 1983: Feasibility test of an airborne pulse-Doppler meteorological radar. *J. Climate Appl. Meteor.,* **22,** 744–757.

——, T. Matejka, and J. D. DuGranrut, 1996: Multi-beam techniques for deriving wind fields from airborne Doppler radars. *Meteor. Atmos. Physics,* **59,** 83–104.

Joss, J., and A. Waldvogel, 1970: Raindrop size distribution and Doppler velocities. Preprints, *14th Conf. on Radar Meteorology,* Tucson, AZ, Amer. Meteor. Soc., 153–156.

Klemp, J. B., 1987: Dynamics of tornadic thunderstorms. *Annu. Rev. Fluid Mech.,* **19,** 369–402.

Lee, W.-C., P. Dodge, F. D. Marks Jr., and P. H. Hildebrand, 1994: Mapping of airborne Doppler radar data. *J. Atmos. Oceanic Technol.,* **11,** 572–578.

Lemon, L. R., 1976: The flanking line, a severe thunderstorm intensification source. *J. Atmos. Sci.,* **33,** 686–694.

——, and C. A. Doswell, 1979: Severe thunderstorm evolution and mesocyclone structure as related to tornadogenesis. *Mon. Wea. Rev.,* **107,** 1184–1197.

Lewellen, W. S., 1993: Tornado vortex theory. *The Tornado: Its Structure, Dynamics, Prediction, and Hazards, Geophys. Monogr.,* No. 79, Amer. Geophys. Union, 19–39.

Markowski, P. M., E. N. Rasmussen, J. M. Straka, and D. C. Dowell, 1998: Observations of low-level baroclinity generated by anvil shadows. *Mon. Wea. Rev.,* **126,** 2942–2958.

——, ——, and ——, 2000: Surface thermodynamic characteristics of RFDs as measured by a mobile mesonet. Preprints, *20th Conf. on Severe Local Storms,* Orlando, FL, Amer. Meteor. Soc., 251–254.

Marwitz, J. D., 1972: The structure and motion of severe hailstorms. Part III: Severely sheared storms. *J. Appl. Meteor.,* **11,** 189–201.

——, and D. W. Burgess, 1994: The observed inflow structure of a thunderstorm with a mesocyclone. *Mon. Wea. Rev.,* **122,** 393–396.

Matejka, T., 2002: Estimating the most steady frame of reference from Doppler radar data. *J. Atmos. Oceanic Technol.,* **19,** 1035–1048.

NCDC, 1995: *Storm Data,* Vol. 37, No. 6, 178–179.

Nelson, S. P., and R. R. Braham Jr., 1975: Detailed observational study of a weak echo region. *Pure Appl. Geophys.,* **113,** 735–746.

Nettleton, L., S. Daud, R. Neitzel, C. Burghart, W. C. Lee, and P.

Hildebrand, 1993: SOLO: A program to peruse and edit radar data. Preprints, *26th Conf. on Radar Meteorology,* Norman, OK, Amer. Meteor. Soc., 338–339.

Oye, R., C. Mueller, and S. Smith, 1995: Software for radar translation, visualization, editing, and interpolation. Preprints, *27th Conf. on Radar Meteorology,* Vail, CO, Amer. Meteor. Soc., 359–361.

Rasmussen, E. N., R. E. Peterson, J. E. Minor, and B. D. Campbell, 1982: Evolutionary characteristics and photogrammetric determination of windspeeds within the Tulia outbreak tornadoes 28 May 1980. Preprints, *12th Conf. on Severe Local Storms,* San Antonio, TX, Amer. Meteor. Soc., 301–304.

——, J. M. Straka, R. Davies-Jones, C. A. Doswell, F. H. Carr, M. D. Eilts, and D. R. MacGorman, 1994: Verification of the Origins of Rotation in Tornadoes Experiment: VORTEX. *Bull. Amer. Meteor. Soc.,* **75,** 995–1006.

Ray, P. S., and M. Stephenson, 1990: Assessment of the geometric and temporal errors associated with airborne Doppler radar measurements of a convective storm. *J. Atmos. Oceanic Technol.,* **7,** 206–217.

——, C. L. Ziegler, W. Bumgarner, and R. J. Serafin, 1980: Single- and multiple-Doppler radar observations of tornadic storms. *Mon. Wea. Rev.,* **108,** 1607–1625.

——, D. P. Jorgensen, and S. L. Wang, 1985: Airborne Doppler radar observations of a convective storm. *J. Climate Appl. Meteor.,* **24,** 687–698.

Rotunno, R., and J. Klemp, 1985: On the rotation and propagation of simulated supercell thunderstorms. *J. Atmos. Sci.,* **42,** 271–292.

Shapiro, A., and J. J. Mewes, 1999: New formulations of dual-Doppler wind analysis. *J. Atmos. Oceanic Technol.,* **16,** 782–792.

Sirmans, D., D. Zrnic, and B. Baumgarner, 1976: Extensions of maximum unambiguous Doppler velocity by use of two sampling rates. Preprints, *17th Conf. on Radar Meteorology,* Seattle, WA, Amer. Meteor. Soc., 23–28.

Speheger, D. A., C. A. Doswell III, and G. J. Stumpf, 2002: The tornadoes of 3 May 1999: Event verification in central Oklahoma and related issues. *Wea. Forecasting,* **17,** 362–381.

Straka, J. M., E. N. Rasmussen, and S. E. Fredrickson, 1996: A mobile mesonet for finescale meteorological observations. *J. Atmos. Oceanic Technol.,* **13,** 921–936.

Trapp, R. J., and C. A. Doswell III, 2000: Radar data objective analysis. *J. Atmos. Oceanic Technol.,* **17,** 105–120.

Wakimoto, R. M., W.-C. Lee, H. B. Bluestein, C.-H. Liu, and P. H. Hildebrand, 1996: ELDORA observations during VORTEX 95. *Bull. Amer. Meteor. Soc.,* **77,** 1465–1481.

——, C. Liu, and H. Cai, 1998: The Garden City, Kansas, storm during VORTEX 95. Part I: Overview of the storm's life cycle and mesocyclogenesis. *Mon. Wea. Rev.,* **126,** 372–392.

Weaver, J. F., and S. P. Nelson, 1982: Multiscale aspects of thunderstorm gust fronts and their effects on subsequent storm development. *Mon. Wea. Rev.,* **110,** 707–718.

Weisman, M. L., and J. B. Klemp, 1982: The dependence of numerically simulated convective storms on vertical wind shear and buoyancy. *Mon. Wea. Rev.,* **110,** 504–520.

——, and ——, 1984: The structure and classification of numerically simulated convective storms in directionally varying wind shears. *Mon. Wea. Rev.,* **112,** 2479–2498.

——, M. S. Gilmore, and L. J. Wicker, 1998: The impact of convective storms on their local environment: What is an appropriate ambient sounding? Preprints, *19th Conf. on Severe Local Storms,* Minneapolis, MN, Amer. Meteor. Soc., 238–241.

Wicker, L. J., 1996: The role of near surface wind shear on low-level mesocyclone generation and tornadoes. Preprints, *18th Conf. on Severe Local Storms,* San Francisco, CA, Amer. Meteor. Soc., 115–119.

Wurman, J., J. M. Straka, and E. N. Rasmussen, 1996: Fine-scale Doppler radar observations of tornadoes. *Science,* **272,** 1774–1777.